The S_3 State of Photosystem II: Differences between the Structure of the Manganese Complex in the S_2 and S_3 States Determined by X-ray Absorption Spectroscopy†

R. D. Guiles,‡,§ J.-L. Zimmermann,‡ Ann E. McDermott,‡,§ Vittal K. Yachandra,‡ James L. Cole,‡,§ S. L. Dexheimer,‡,∥ R. D. Britt,‡,∥ Karl Wieghardt,⊥ Ursula Bossek,⊥ Kenneth Sauer,‡,§ and Melvin P. Klein*,‡

Laboratory of Chemical Biodynamics, Lawrence Berkeley Laboratory, and Departments of Chemistry and Physics, University of California, Berkeley, California 94720, and Ruhr-Universität-Bochum, Lehrstuhl für Anorganische Chemie I, 4630 Bochum-Querenburg, FRG

Received December 20, 1988; Revised Manuscript Received August 16, 1989

ABSTRACT: O_2-evolving photosystem II (PSII) membranes from spinach have been cryogenically stabilized in the S_3 state of the oxygen-evolving complex. The cryogenic trapping of the S_3 state was achieved using a double-turnover illumination of dark-adapted PSII preparations maintained at 240 K. A double turnover of PSII was accomplished using the high-potential acceptor, Q_{400}, which is the high-spin iron of the iron–quinone acceptor complex. EPR spectroscopy was the principal tool establishing the S-state composition and defining the electron-transfer events associated with a double turnover of PSII. The inflection point energy of the Mn X-ray absorption K-edge of PSII preprarations poised in the S_3 state is the same as for those poised in the S_2 state. This is surprising in light of the loss of the multiline EPR signal upon advancing to the S_3 state. This indicates that the oxidative equivalent stored within the oxygen-evolving complex (OEC) during this transition resides on another intermediate donor which must be very close to the manganese complex. An analysis of the Mn extended X-ray absorption fine structure (EXAFS) of PSII preparations poised in the S_2 and S_3 states indicates that a small structural rearrangement occurs during this photoinduced transition. A detailed comparison of the Mn EXAFS of these two S states with the EXAFS of four multinuclear μ-oxo-bridged manganese compounds indicates that the photosynthetic manganese site most probably consists of a pair of binuclear di-μ-oxo-bridged manganese structures. However, we cannot rule out, on the basis of the EXAFS analysis alone, a complex containing a mononuclear center and a linear trinuclear complex. The subtle differences observed between the S states are best explained by an increase in the spread of Mn–Mn distances occurring during the $S_2 \rightarrow S_3$ state transition. This increased disorder in the manganese distances suggests the presence of two inequivalent di-μ-oxo-bridged binuclear structures in the S_3 state.

The current model of photosynthetic oxygen evolution carried out by higher plants and cyanobacteria involves five intermediate oxidation states, commonly referred to as S states: S_0–S_4 (Kok et al., 1970). This model is based on the remarkable observation made by Joliot et al. (1969) that the production of O_2 by dark-adapted chloroplasts subjected to a series of short saturating flashes of light occurs in distinct pulses with a periodicity of four. The states S_0, S_1, S_2, and S_3 are relatively stable intermediate oxidation states of the oxygen-evolving complex (OEC).[1] The S_4 state is a transient intermediate and decays to produce the S_0 state, concurrent with the release of O_2. The S_1 state is predominant in long-term dark-adapted PSII preparations. An abundance of physical and biochemical evidence indicates that a cluster of manganese located within a membrane-bound protein–chlorophyll complex is the site where the light-driven oxidation of water to molecular oxygen takes place [for a review, see Babcock (1987)].

The first physical evidence implicating a manganese cluster in the water oxidation process in catalytically active chloroplast preparations came from the discovery of a light-induced multiline EPR signal assigned to a manganese complex because of its characteristic hyperfine structure. The multiline EPR signal was associated with the S_2 state, on the basis of the variation in its amplitude observed with flash number (Dismukes & Siderer, 1981). A large number of studies have now been performed, extensively characterizing the S_2 state using the multiline EPR signal. On the other hand, there have been relatively few reports of attempts to stabilize active O_2-evolving preparations cryogenically in the S_3 state (Brudvig et al., 1983;

† This work was supported by a grant from the National Science Foundation (PCM 84-16676) and by the Director, Office of Energy Research, Office of Basic Energy Sciences, Division of Biological Energy Research of the U.S. Department of Energy under Contract DE-AC03-76SF00098. Synchrotron radiation facilities were provided by the Stanford Synchrotron Radiation Laboratory, which is supported by the Office of Basic Energy Sciences, U.S. Department of Energy, and by the NIH Biotechnology Program, Division of Resources. J.-L.Z. is supported by the Commissariat à l'Energie Atomique (France) and by a grant from NATO (108C86FR). This is paper 10 in the series "The State of Manganese in the Photosynthetic Apparatus".

* To whom correspondence should be addressed.

‡ Laboratory of Chemical Biodynamics, Lawrence Berkeley Laboratory, University of California.

§ Department of Chemistry, University of California.

∥ Department of Physics, University of California.

⊥ Ruhr-Universität-Bochum.

[1] Abbreviations: cyt b_{559}, cytochrome b_{559}; DCBQ, 2,6-dichloro-*p*-benzoquinone; DCMU, 3-(3,4-dichlorophenyl)-1,1-dimethylurea; DMSO, dimethyl sulfoxide; EPR, electron paramagnetic resonance; EXAFS, extended X-ray absorption fine structure; MES, 4-morpholineethanesulfonic acid; MLS, multiline signal; OEC, oxygen-evolving complex; PPBQ, phenyl-*p*-benzoquinone; PSII, photosystem II; Q_{400}, the high-potential acceptor of PSII; tacn, 1,4,7-triazacyclononane.

0006-2960/90/0429-471$02.50/0

Goodin et al., 1984). As yet, no spectroscopic signal uniquely characteristic of the S_3 state has been discovered. As a result, previous studies relied upon decreases in the amplitude of the multiline EPR signal as an indication of advancement to the S_3 state following a single turnover by low-temperature illumination of samples poised initially in the S_2 state.

Here, we report experiments poising samples predominantly in the S_3 state by a double-turnover, low-temperature illumination of samples where Q_{400} was initially present in the oxidized form. The chemical identity of the high-potential (E_m = 370 mV at pH 7.5) acceptor, Q_{400}, has been established as the high-spin iron of the iron–quinone acceptor complex of PSII (Petrouleas & Diner, 1986). We produced oxidized Q_{400} either by direct chemical oxidation using ferricyanide (Petrouleas & Diner, 1986) or by photoreductant-induced oxidation through the use of phenyl-*p*-benzoquinone (PPBQ) (Zimmermann & Rutherford, 1986). Low-temperature illumination of PSII preparations in which oxidized Q_{400} was produced by either of these procedures was found to produce substantial S_3 state yields. The photochemical events occurring during the procedure used to accumulate the S_3 state were monitored by recording the EPR signals associated with $Q_A^-Fe^{2+}$ and with the high-spin Fe^{3+} associated with oxidized Q_{400}. The final S-state composition was deduced from these measurements and from the amplitude of the multiline signal relative to controls limited to a single turnover of PSII, as well as from the magnitude of EPR signals arising from alternate donors such as cyt b_{559}.

X-ray absorption spectroscopy has been demonstrated to yield detailed information about the local structure of a metalloenzyme and does not require a crystalline sample (Powers, 1982; Teo, 1986). Further, the accuracy of the distance information obtained from multiparameter fitting of extended X-ray absorption fine structure (EXAFS) is significantly better than that obtainable from X-ray diffraction studies of proteins, and the sensitivity of the technique to changes in the local structure of a metalloenzyme has been demonstrated to be of utility in deducing important details of the mechanism of enzyme activity (Eisenberger & Kincaid, 1978). With the multiline EPR signal as a monitor of state composition, the direct involvement of manganese in the storage of oxidative equivalents on the donor side of photosystem II has been demonstrated by using Mn X-ray absorption edge spectroscopy (Goodin et al., 1984). The ligation sphere of manganese in the S_1 and S_2 states has also been probed with EXAFS (Yachandra et al., 1986, 1987; McDermott et al., 1988).

In this report we present the results of X-ray absorption experiments performed on samples poised predominantly in the S_3 state. By contrast with our previous studies of the $S_1 \rightarrow S_2$ state transition (Goodin et al., 1984; Yachandra et al., 1987), no change was observed in the edge position or structure of the Mn X-ray absorption K-edge upon state advancement from S_2 to S_3. Results presented in the present study using PSII subchloroplast membrane preparations largely confirm our previous report of a Mn K-edge study (Goodin et al., 1984), indicating that the Mn X-ray absorption K-edges of chloroplast preparations poised in the S_2 and S_3 states are observed at higher X-ray energies than that of samples poised in the S_1 state. EXAFS analyses of PSII preparations cryogenically stabilized in the S_2 and S_3 states indicate that a small structural change occurs at the manganese site in PSII during the $S_2 \rightarrow S_3$ state transition. The X-ray absorption data presented here are of significantly improved signal-to-noise ratio compared to those we have previously published for the S_1 and S_2 states, due principally to improvements in fluorescence detection. The present analysis largely confirms our previous conclusions of the presence of a di-μ-oxo-bridged Mn binuclear core structure present in the S_2 state (Yachandra et al., 1986, 1987; McDermott et al., 1988). Conclusions are drawn from a detailed comparison of the simulation results obtained for four multinuclear manganese compounds with results obtained for the PSII preparations, and the significance of these analyses to other results and models of the water oxidation mechanism already published in the literature is discussed.

Materials and Methods

PSII Subchloroplast Membrane Preparation and Handling. The procedure for isolation of active O_2-evolving PSII subchloroplast membranes from market spinach has been described by Yachandra et al. (1986). Single- or double-turnover experiments using DCBQ (Eastman), PPBQ (Eastman), or DCMU (Sigma) were performed by adding a calculated volume of a DMSO stock solution of the given reagent to PSII membranes suspended at 2 mg/mL chlorophyll. Chemical oxidation of cyt b_{559} and Q_{400} was accomplished by incubating PSII membranes suspended at 3 mg/mL chlorophyll in the dark for 10 min in a buffer containing 5 mM $K_3Fe(CN)_6$, 15 mM NaCl, 5 mM $MgCl_2$, and 50 mM MES (pH = 6.5). To obtain the manganese concentrations required for the X-ray absorption experiments, the PSII membrane suspensions were centrifuged at 30000*g* for 1 h. Pellets containing approximately 30% glycerol were transferred to Lucite sample holders. Chlorophyll concentrations in samples prepared for X-ray absorption experiments ranged from 25 to 30 mg/mL.

Low-temperature illumination or equilibration was accomplished in an optical Dewar cooled by a N_2 gas stream; the sample was maintained at a constant temperature by a Varian V6040 temperature controller. Samples were mounted directly into Lucite sample holders that were designed to fit into the liquid He cryostat associated with the EPR spectrometer as well as the cooled N_2 gas flow cryostat used for the X-ray absorption experiments. All illuminations, constant-temperature equilibrations, EPR measurements, and X-ray absorption measurements were performed on samples mounted in this manner.

EPR Spectra. Low-temperature X-band EPR spectra were recorded by using a Varian E109 EPR spectrometer equipped with an E-102 microwave bridge and an Air Products LTR liquid helium cryostat. The temperature of the sample was monitored by using a gold–chromel thermocouple junction. EPR spectra were digitized by using an Explorer III storage oscilloscope (Nicolet Instrument Corp., Madison, WI) and then transferred to a VAX 11-785 computer for further analysis. Separate EPR spectra were recorded for each electron-transfer component of interest under conditions that maximized the EPR signal amplitude. Exact spectrometer conditions for each EPR signal are indicated in the figure captions. The magnitude of the g = 4.3 EPR signal, associated with adventitiously bound iron, was used as an internal calibration reference when comparing two different samples. The amplitude of this feature in dark-adapted samples was found to differ less than 5% between samples from the same preparation. Mulitline EPR signal amplitudes were quantitated by adding peak-to-trough amplitudes of four of the low-field hyperfine lines from illuminated-minus-dark difference spectra. The Q_{400} signal was quantitated by measuring the peak to base line amplitudes of the lowest field component near g = 8. The amplitude of the reduced quinone acceptor, $Q_A^-Fe^{2+}$, was determined from the peak-to-trough difference of the g = 1.9 EPR signal observed in the illuminated samples, for it was

found that in the PSII preparations used in this study the dominant EPR signal characteristic of the $Q_A^-Fe^{2+}$ complex was the $g = 1.9$ feature (Rutherford & Zimmermann, 1984). Signal II_s, which is present in the dark and associated with D^+, a donor to PSII with unknown function, was quantitated by measuring peak-to-trough amplitudes between the two outermost hyperfine lines. The amplitude of oxidized cyt b_{559} was determined by measuring the peak to base line amplitudes of the $g = 3.0$ feature.

Inorganic Manganese Compounds. Four structurally characterized inorganic multinuclear manganese compounds were examined in this study. The four inorganic compounds examined were $Mn^{III}Mn^{IV}(\mu_2\text{-}O)_2(2,2'\text{-bipyridine})_4(ClO_4)_3$ (**1**) (Plaskin et al., 1972), $Mn^{IV}_2(\mu_2\text{-}O)_2(\text{picolinate})_4$ (**2**), $Mn^{IV}_4(\mu_2\text{-}O)_6(\text{tacn})_4(ClO_4)_4$ (**3**) (Wieghardt & Bossek, 1983), and $Mn^{III}_4(\mu_3\text{-}O)_2(OAc)_7(2,2'\text{-bipyridine})_2(ClO_4)$ (**4**) (Vincent et al., 1987). Complex **2** was synthesized and characterized in the laboratory of Dr. G. Christou. Manganese compounds will be referred to in the text by the boldface number indicated. Solid samples were diluted into an inert light-element matrix ($LiBF_4$ or Li_2CO_3) and mounted in Lucite sample holders.

X-ray Absorption Measurements. X-ray absorption spectra were recorded at the Stanford Synchrotron Radiation Laboratory on wiggler beam lines IV-2 and VI-2 using a Si⟨400⟩ double-crystal monochromator. The energy resolution of these crystals is approximately 1 eV. X-ray absorption edge spectra were recorded by using a fluorescence detection system (Jaklevic et al., 1977) similar to that described by Powers et al. (1981). It consisted of an array of NE104 plastic scintillators coupled to EMI 9813 B photomultiplier tubes. The fluorescence detector was equipped with a chromium filter and Soller slit assembly (Stern & Heald, 1979). The fluorescence signal was ratioed to a measure of the incident flux, which was monitored by an additional scintillator. This scintillator viewed the flux of X-rays scattered from a thin mylar film which was placed directly in the incident X-ray beam. This method of ratioing yielded a much more linear response than the ionization chamber method previously employed.[2]

EXAFS spectra of the PSII preparations were collected by using a lithium-drifted silicon solid-state detector as previously described (Jaklevic et al., 1977). Count rate capabilities of this detection system were substantially enhanced through the use of a triangular pulse shaping amplifier (Goulding et al., 1983). The use of an energy-resolving detector capable of efficient background rejection significantly improved the signal-to-noise ratio of these spectra over previously published results (Yachandra et al., 1987). All samples were maintained at or below 190 K in a home-built double Kapton-walled cryostat, cooled by a nitrogen gas flow system. To assure sample integrity and a stable S-state composition, EPR spectra of the PSII samples were monitored before and after exposure to the X-ray beam. Energy calibration in the X-ray absorption experiments was maintained by simultaneously monitoring the narrow preedge feature of a $KMnO_4$ standard (Goodin et al., 1979). Typically, one scan (3 s per point) yielded satisfactory signal-to-noise ratios for the model complexes. To achieve the signal-to-noise ratio presented here for the PSII preparations, 10–30 scans were averaged.

Data Analysis. All analyses of the X-ray absorption spectra were performed on a VAX 11/785. The region below the onset of manganese X-ray absorption was set equal to zero by subtracting a linear fit to the spectrum below the edge. Spectra were normalized to a unit edge jump determined by extrapolation of a quadratic fit of the postedge absorption to the energy of the first major absorption peak. The magnitude of this extrapolated fit at the energy of the first major absorption peak was set equal to one. Details of the analysis of the EXAFS data have been described previously (Yachandra et al., 1986, 1987).

Detailed structural information regarding the number of ligands and the distances to these ligands is obtained by fitting the EXAFS data to the known functional form of these waves. Commonly, either theoretically calculated phase and amplitude functions (Teo & Lee, 1979) or empirical phase and amplitude functions derived from structurally similar model complexes (Cramer et al., 1976) were used in these simulations. Here, we have taken the former approach; however, adjustments based on a set of crystallographically characterized multinuclear manganese compounds were used to refine the information obtained from the fits (Teo et al., 1983). It is important to note that EXAFS analyses that have been adjusted on the basis of models become "model dependent", so the method of selection of the inorganic complexes of known structure used as models becomes an important part of the procedure. Teo et al. (1983) have suggested several selection criteria that involve comparisons between the unknown and the model with regard to variations of the apparent scatterer distances with changes in K-edge energy and changes in the apparent number of scatterers as a function of the Debye–Waller magnitude. Procedures employing empirically derived amplitude and phase functions clearly are also model dependent at a much earlier level in the analysis procedure.

Under favorable conditions, distances accurate to ±0.03 Å and determinations of the number of scatters to within 20% of crystallographically determined values are obtained. The energy of the absorption edge is allowed to vary in simulations using theoretically derived phase functions to allow better phase matching to the experimental waves. In this study, the variation of this parameter, ΔE_0, was constrained to values between 0 and −20 eV for the light scatterers and to between 0 and −10 eV for the manganese neighbor, for it was found that simulations in closest agreement with the crystallographic distances were obtained with ΔE_0 values in these ranges. Manganese–manganese distances obtained from an EXAFS analysis of multinuclear μ-oxo-bridged manganese complexes were found to be within ±0.03 Å of the crystallographically determined distances when these constraints on the range of variation in the edge threshold were applied. On the basis of calculated Debye–Waller factors for inorganic compounds exhibiting similar parameter correlations, the Debye–Waller factors for each scattering shell of the PSII preparations were constrained to reasonable values to reduce the uncertainty in the number of scatterers. Also, scale factors that improve the accuracy of the determination of the number of atoms in a given shell of the PSII preparation were determined from these inorganic compounds. Scale factors were calculated from the ratio of the simulated number of scatterers in a given shell to the number of atoms at a given distance from the absorbing atom determined from the crystal structure of the inorganic compound.

Uncertainties in the number of scatterers due to the effect of correlation with the Debye–Waller factor were calculated by systematically varying the number of scatterers from the best fit value. Calculated uncertainties represent values for the number of scatterers in which the least-squares residual was twice the minimum value. All variables except the Debye–Waller factor were constrained to the best fit value during

[2] This method of ratioing was first suggested to us by Prof. B. Chance (personal communication).

Scheme I: PPBQ Procedure for the Preparation of a PSII Sample Poised in the S_3 State[a]

sample preparation procedure	state of the system
step 1: dark adapt 1 h	S_1(cyt b_{559})Q_AFe^{2+}PPBQ
step 2: illuminate at 77 K for 1 h	S_1(cyt b_{559}^+)$Q_A^-Fe^{2+}$PPBQ
step 3: warm to 293 K for 1 min	S_1(cyt b_{559}^+)Q_AFe^{2+}PPBQ$^-$
	S_1(cyt b_{559}^+)Q_AFe^{3+}PPBQH$_2$
step 4: illuminate at 240 K for 10 min	S_3(cyt b_{559}^+)$Q_A^-Fe^{2+}$PPBQH$_2$

[a] The oxidation state of the electron-transfer components within PSII indicated on the first line of Step 3 is intended to represent an unstable intermediate state involving the transient PPBQ semiquinone which presumably is formed prior to the oxidation of the acceptor iron.

these simulations. Clearly, the presence of random noise in the spectra also limits the accuracy of the amplitudes of EXAFS waves which, when simulated, yield estimates of the number of scatterers. A conservative estimate of the root-mean-square noise level in a Fourier transformed data set (Ernst et al., 1987) may be determined by taking the average amplitude of Fourier peaks well beyond the region where real components are observed. In this case the region between 6 and 15 Å was used to determine the average amplitude of noise peaks. For the k^3-weighted S_2 state EXAFS data, the average amplitude is approximately 20% of the amplitude of the two clearly resolved shells. Assuming that the effects of parameter correlation and random noise act independently, the combined effects of these sources of uncertainty should be given by their quadrature sum. Given that the effect of parameter correlations with the Debye–Waller term also limit the accuracy of the number of scatterers to ±20% under favorable circumstances (e.g., for the oxygen shell at the shortest apparent distance and the Mn shell of the PSII preparations poised in the S_2 state), these combined effects limit the accuracy to ±30% of the best fit value.

For the S_3 state data the signal-to-noise ratio is substantially smaller due to the necessity of employing a difference technique. For these data the average amplitude of features in the Fourier transform in the range of 6–15 Å is on the order of 40%. Combined with a larger error due to correlation with the Debye–Waller term for the Mn shell, the error in the number of scatterers is estimated to be closer to ±60% and ±50% for the short bond length oxygen shell.

Results

O_2-evolving PSII samples suitable for X-ray spectroscopy and poised in the S_3 state were prepared by a low-temperature illumination of dark-adapted PSII preparations in which Q_{400} had been oxidized (i.e., the high-spin iron of the acceptor complex had been oxidized to Fe^{3+}). Two protocols based on recently published results concerning the generation of oxidized Q_{400} and its subsequent photoreduction were used in this study: Petrouleas and Diner (1986) oxidized Q_{400} using a ferricyanide treatment of PSII membranes in the dark. EPR signals associated with oxidized Q_{400} were identified in the region near $g = 8$ and $g = 5.5$. Zimmermann and Rutherford (1986) found that addition of 1 mM PPBQ to a PSII subchloroplast membrane suspension can also result in the oxidation of Q_{400} following a low-temperature illumination and subsequent warming. We have employed both the ferricyanide oxidation and the PPBQ-mediated oxidation procedure for the generation of oxidized Q_{400}. Each procedure was found to have certain advantages in the double-turnover illumination procedure used to generate samples poised predominantly in the S_3 state.

PPBQ Experiments. A schematic representation of the dominant electron-transfer steps yielding a PSII preparation poised predominantly in the S_3 state using PPBQ is presented

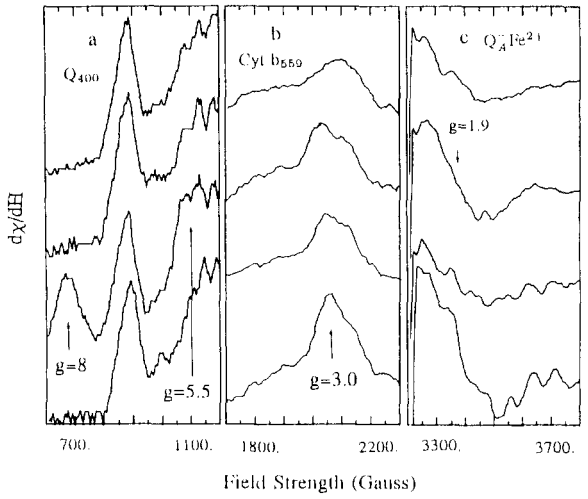

FIGURE 1: Changes in the EPR spectra of (a) Q_{400}, (b) cyt b_{559}^+, and (c) $Q_A^-Fe^{2+}$, which are observed for PSII preparations during the course of the S_3 state preparation procedure using PPBQ. In each panel the EPR spectra shown from top to bottom are as follows: a dark-adapted PSII preparation, the same sample following illumination at 77 K for 1 h, the preceding sample following warming for 1 min at 293 K, and (bottom spectrum) this sample following illumination at 240 K for 10 min. Spectrometer conditions: (a and c) 32-mW microwave power at 9.21 GHz, 32-G field modulation at 100 kHz, recorded at 5 K; (b) 0.2-mW microwave power at 9.21 GHz, 20-G field modulation at 100 kHz, recorded at 18 K.

in Scheme I. The steps in the experiment in which PPBQ was used to oxidize Q_{400} and leading to a PSII preparation containing a substantial S_3 state composition are as follows: (1) long-term (>1-h) dark adaptation followed by addition in the dark of a calculated volume of a PPBQ stock solution which brought the suspension to 1 mM; (2) illumination at 77 K for a period of 1 h; (3) warming samples for 1 min at 293 K; and (4) illumination at 240 K for 10 min. The electron-transfer events described below were monitored by examining changes in the amplitudes of EPR signals associated with each electron-transfer component.

Illumination of dark-adapted PSII membranes at 77 K results in the photoaccumulation of $Q_A^-Fe^{2+}$ largely at the expense of cyt b_{559} oxidation. These events were monitored by EPR spectroscopy. Figure 1 shows the EPR spectra of cyt b_{559}^+ and $Q_A^-Fe^{2+}$, which were induced by this process. Warming of such a sample containing PPBQ in the dark results in the reoxidation of Q_A^- and oxidation of the ferrous ion (step 3 in Scheme I) in a process that was first demonstrated by Zimmermann and Rutherford (1986) and later confirmed by Petrouleas and Diner (1987). These results were largely confirmed in this study, and Figure 1 shows that following the warming step the $Q_A^-Fe^{2+}$ signal decays to its original amplitude, demonstrating the complete reoxidation of the primary quinone acceptor. The oxidation of Fe^{2+} (i.e., the formation of oxidized Q_{400}) is indicated by well-resolved features near $g = 8$ and $g = 5.5$ (Figure 1a).

Zimmermann and Rutherford (1986) showed that significant amounts of oxidized Q_{400} could be induced in the dark by the addition of PPBQ to dark-adapted PSII membranes (presumably by oxidizing the amount of Q_B^- present in the dark). To avoid this side reaction which would affect the final S-state composition, Q_B^- was oxidized before the PPBQ treatment by the addition of 50 μM DCBQ. As observed by Zimmermann and Rutherford (1986), DCBQ does not induce the oxidation of Fe^{2+}, and the absence of high-spin iron signals associated with Q_{400} in the spectrum shown in Figure 1a shows that the addition of PPBQ after this treatment effectively suppressed the generation of Q_{400} in the dark.

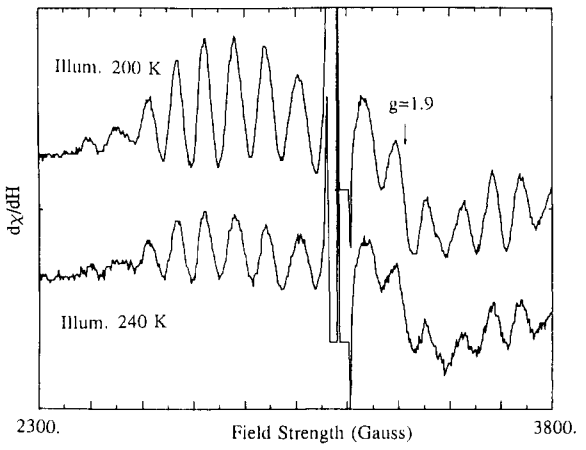

FIGURE 2: Illuminated-minus-dark EPR spectra of the multiline signal in the control S_2 state preparation generated by illumination at 200 K (top trace) and a PSII preparation poised partially in the S_3 state by the procedure employing PPBQ (bottom trace). The S_3 state preparation was generated by illumination at 240 K. Spectrometer conditions: 32-mW power at 9.21 GHz, 32-G field modulation at 100 kHz, recorded at 8 K.

Table I: Changes in the EPR Signal Amplitudes[a] of Electron-Transfer Components of PSII Observed during the S_3 Preparation Procedure Using PPBQ

sample preparation	MLS (%)	$Q_A^-Fe^{2+}$ (%)	Q_{400}	cyt b_{559}
step 1: dark adapt 1 h	<5	<10	<2	6.5
step 2: illuminate at 77 K	<5	90	<2	11.0
step 3: warm to 293 K	12[b]	<10	19	10.0
step 4: illuminate at 240 K	54	110	<2	16.0

[a] All amplitudes reported here are in arbitrary units. Percentages reported are the MLS and $g = 1.9$ feature of the EPR signal associated with $Q_A^-Fe^{2+}$, observed in S_2 control preparations. Exact details of the quantitation are described under Materials and Methods. [b] The small amount of MLS generated during the warming step is presumably due to the conversion of the amount of the $g = 4.1$ species (formed at 77 K) to the S_2 state characterized by the MLS [see Casey and Sauer (1984)].

Several changes in the EPR spectra of the PSII preparations following the final period of illumination at 240 K are indicative of a double turnover of PSII: (1) the $Q_A^-Fe^{2+}$ signal at $g = 1.9$ is induced to virtually the same extent as after the illumination at 77 K, indicating one complete charge separation in the final illumination (Figure 1c), and (2) the EPR signals at $g = 8$ and $g = 5.5$ associated with Q_{400} disappear (Figure 1a), indicating the reduction of Fe^{3+} to Fe^{2+} and the stabilization of a second oxidative equivalent on the donor side of photosystem II. Thus, since both Q_A and Q_{400} were reduced during this final illumination, we conclude that the PSII reaction center underwent a double turnover, resulting in the stabilization of two oxidizing equivalents on the donor side of PSII.

As shown in Figure 1b, the amplitude of the EPR signal of cyt b_{559} increases by 50% during the illumination at 240 K. Because cyt b_{559} does not compete with S_1 state donation at this temperature, it is concluded that cyt b_{559} photooxidation competed with S_2 state donation during the second turnover. Quantitation of the EPR signal indicates that 0.5 cyt was oxidized. Thus, the remaining 50% of the centers underwent a double turnover involving S-state donation, resulting in the accumulation of the S_3 state. This interpretation is in agreement with the amount of multiline signal photoinduced during the last step (step 4 of Scheme I), which corresponds to 50% of the amplitude photoinduced in a sample prepared by illumination at 200 K (Figure 2). The results are summarized in Table I.

Scheme II: Ferricyanide Procedure for the Preparation of a PSII Sample Poised in the S_3 State

sample preparation procedure	state of the system
step 1: dark adapt 1 h	S_1(cyt b_{559})$Q_AFe^{2+}Q_B$
step 2: add 5 mM ferricyanide; incubate for 10 min at pH 6.5	S_1(cyt b_{559}^+)$Q_AFe^{3+}Q_B$
step 3: add 200 μM DCMU	S_1(cyt b_{559}^+)Q_AFe^{3+}DCMU
step 4: illuminate at 240 K for 10 min	S_3(cyt b_{559}^+)$Q_A^-Fe^{2+}$DCMU

Table II: Changes in the EPR Signal Amplitudes[a] of Electron-Transfer Components of PSII Observed during the S_3 Preparation Procedure Using Ferricyanide

sample preparation procedure	MLS (%)	Q_{400}	cyt b_{559}
step 1: dark adapt 1 h	<5	<2	<2[b]
step 2: ferricyanide oxidation	<5	15[c]	26[c]
step 3: DCMU washed	<5	16	11
step 4: illuminate at 240 K	34	<2	12

[a] All amplitudes reported here are in arbitrary units. Percentages reported for the MLS are relative to the control S_2 state preparation. Exact details of the quantitation are described under Materials and Methods. [b] The amplitude reported for the dark sample is that of low-potential cytochrome b_{559}, which is normally oxidized at the ambient potential of the preparation. The amplitude of this signal is near the uncertainty in the measurement of the $g = 3.0$ feature (e.g., ± 1). [c] EPR signal amplitudes of Q_{400} and cyt b_{559} found in controls in which ferricyanide was retained.

One additional property of PSII preparations poised in the S_3 state by the PPBQ procedure allowed the preparation of a "thermally relaxed" S_3 state sample. The dominant effect observed upon warming a PSII preparation poised in the S_3 state by the PPBQ procedure was forward electron transfer and subsequent reoxidation of Q_{400} (a repetition of the acceptor side reaction indicated in step 3 of Scheme I). These events were evident from the lack of change in the amplitude of the multiline EPR signal and the disappearance of the $g = 1.9$ EPR signal, indicating reoxidation of Q_A^- (spectra not shown).

Ferricyanide Experiments. In the second procedure used to generate PSII preparations poised in the S_3 state, Q_{400} was oxidized by ferricyanide before the double-turnover illumination. The dominant electron-transfer events occurring during this procedure are depicted in Scheme II. The protocol used is summarized as follows: (1) Long-term (>1-h) dark adaptation; (2) ferricyanide oxidation of Q_{400} in the dark with concurrent oxidation of cytochrome b_{559}; and (3) illumination for 10 min at a temperature above the threshold (235 K) for advancement to the S_3 state (Brudvig et al., 1983).

An additional step (step 3 in Scheme II) was incorporated into the procedure to ensure that PSII was limited to two turnovers. DCMU, which blocks electron transfer between Q_A and Q_B, was added to the preparation after the treatment with 5 mM ferricyanide. PSII suspensions were washed in the dark with a MES buffer (pH = 6.5) containing 200 μM DCMU, effectively washing out the ferricyanide used in the previous step. This step eliminated concerns about possible leakage of electrons from $Q_A^-Fe^{2+}$ through the DCMU block to the ferricyanide in the aqueous phase and removed the interference due to the broad and intense ferricyanide signal centered at $g = 2$, which obscures the reduced quinone signals at $g = 1.9$ and $g = 1.82$. Samples treated in this manner were used in the X-ray absorption experiments.

Control experiments were also performed in which the 5 mM ferricyanide was retained during the DCMU wash step. These controls were important in evaluating whether Q_{400} and high-potential cyt b_{559} remain oxidized at the ambient potential attained after the ferricyanide is removed. Table II contains the amplitudes of the EPR signals associated with Q_{400} and oxidized cyt b_{559} at each step of the process leading to a PSII

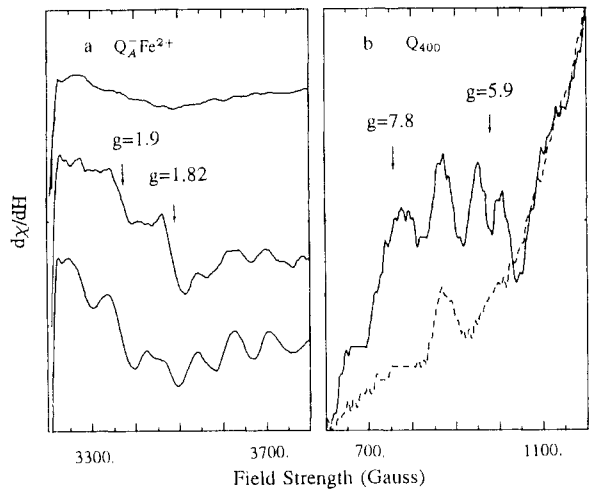

FIGURE 3: EPR signals associated with the PSII acceptors $Q_A^-Fe^{2+}$ and Q_{400}. The spectra shown in (a) are as follows: The top trace is the spectrum of a PSII preparation dark adapted for 1 h, treated with 5 mM ferricyanide in the dark for 10 min, and then subsequently washed free of ferricyanide with a pH = 6.5 MES buffer containing 200 μM DCMU. The second trace from the top is the same sample following illumination at 240 K. The lower trace is the spectrum of the control S_2 state sample prepared by illumination at 195 K. Spectrometer conditions are the same as for the spectra shown in Figure 1c. The spectra shown in (b) are of the low-field region of the EPR spectrum of PSII preparations recorded at 5 K. The solid trace is the spectrum of a dark-adapted PSII preparation treated with 5 mM ferricyanide in the dark. The dashed line is the spectrum of the same PSII preparation following illumination at 240 K. Spectrometer conditions are the same as for Figure 1a.

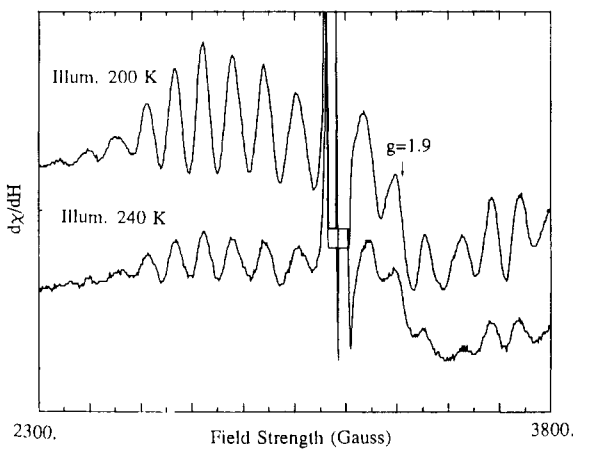

FIGURE 4: Illuminated-minus-dark EPR spectra of the multiline signal in the control S_2 state preparation generated by illumination at 200 K (top trace) and a PSII preparation poised partially in the S_3 state by the ferricyanide procedure (bottom trace). The S_3 state preparation was generated by illumination at 240 K. The state composition indicated by the fraction of the residual multiline in the lower spectrum is 66% S_3 and 34% S_2. EPR spectrometer conditions are the same as for Figure 2.

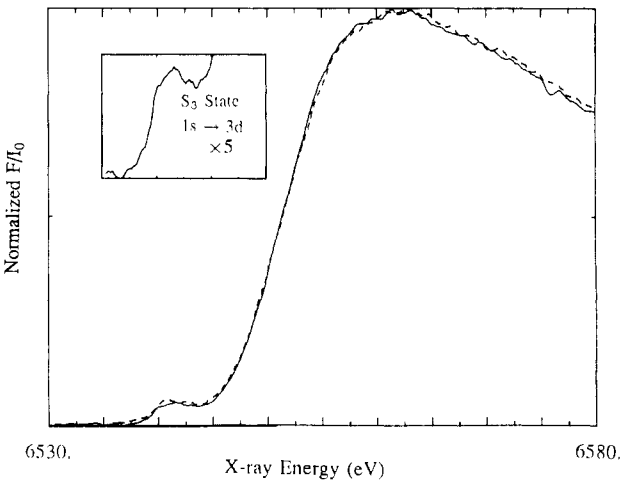

FIGURE 5: Mn K-edge X-ray absorption spectrum of a PSII preparation poised in the S_2 state (---) and a preparation poised predominantly in the S_3 state (—) using the ferricyanide procedure. Spectra were smoothed by using a quadratic running fit with a smoothing domain of 2 eV. The inset is a 5× magnification of the 1s → 3d transition of the X-ray absorption spectrum of a PSII preparation poised in the S_3 state.

sample poised in the S_3 state using the ferricyanide procedure. Note that the amplitudes of the g = 8 feature in the EPR spectrum of Q_{400} observed in samples in which the ferricyanide was washed out are at the same level, or somewhat higher, than the amplitude of this feature in samples in which the ferricyanide was retained. This indicates that the rereduction of oxidized Q_{400} at the ambient potential achieved after the ferricyanide is removed is kinetically limited. Table II shows also that the amplitude of the g = 3.0 feature associated with oxidized cyt b_{559} in the 18 K spectra of the samples retaining ferricyanide is significantly higher than the amplitude of this feature in the samples in which the ferricyanide was washed out. However, it is important to note that the amplitude of the cytochrome EPR signal remained relatively constant during the final illumination step. This demonstrates that photoinduced oxidation of cyt b_{559} was not a significant side reaction at the temperatures utilized.

The effect of illumination following the dark oxidation was examined at three different temperatures: 250, 245, and 240 K. The reduction in the amplitude of the multiline signal relative to that of the control 195 K illumination is relatively constant (57–66%) across the range of temperatures of illumination examined. The maximum S_3 state composition was achieved at the lowest temperature of illumination (Figure 2). Also, the magnitude of the reduction of the MLS relative to the controls was consistently larger than that obtained in the PPBQ experiments. This is due principally to the elimination of competitive donation by cytochrome b_{559}.

Figure 3 shows the 5 K EPR spectra of the ferricyanide-oxidized PSII sample before and after illumination at 240 K. The salient spectral changes associated with the transfer of 2 equiv to the acceptor side and the generation of a PSII preparation poised predominantly in the S_3 state are evident from these two spectra. The large increase in the g = 1.9 region and the disappearance of signals in the g = 8 and g = 5.5 regions of the EPR spectra recorded at 5 K indicate near quantitative reduction of Q_A and Q_{400}, respectively (see Figure 3). The amplitude of the multiline signal present indicates a state composition containing 34% S_2 (see Figure 4).

X-ray Absorption Edge Studies. Figure 5 contains a representative Mn K-edge spectrum of an S_3 sample together with that of a control S_2 state preparation. The Mn K-edge shown is that of an S_3 state preparation generated by illumination at 240 K using the ferricyanide procedure. In addition to the ferricyanide samples, a sample poised in the S_3 state by the PPBQ procedure and subsequently warmed to room temperature for 30 s to allow thermal equilibration was examined. The energy of the Mn K-edge inflection for all of the S_2 and S_3 samples studied here was found to be within 0.2 eV of 6552.1 eV. The edge shape and the energy of the Mn K-edge inflection of the S_2 and S_3 state preparations are remarkably similar. The energy of the Mn K-edge inflection and the similarity of the 1s → 3d transition both are indicative of the presence of Mn(IV) (Sauer et al., 1988; Guiles, 1988). The low-intensity feature at energy lower than the edge inflection is due to X-ray transitions of principally 1s → 3d character.

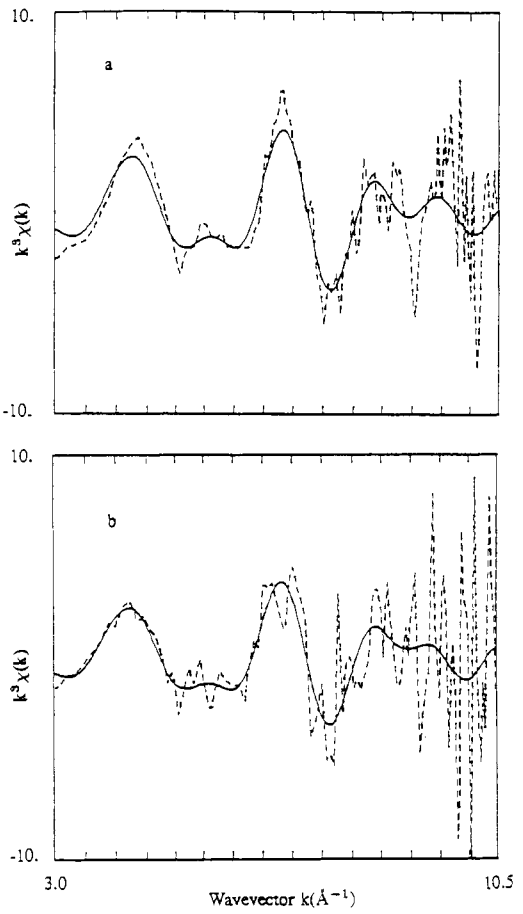

FIGURE 6: EXAFS region of the Mn X-ray absorption spectrum of PSII preparations poised (a) in the S_2 state and (b) in the S_3 state. The spectrum in (b) is the difference EXAFS spectrum of a PSII preparation poised predominantly in the S_3 state by the ferricyanide procedure from which a fraction of the control S_2 state preparation EXAFS has been subtracted. The data are indicated with a dashed line, and the solid line represents the contribution from the two main peaks in the Fourier transform of the EXAFS shown in Figure 7.

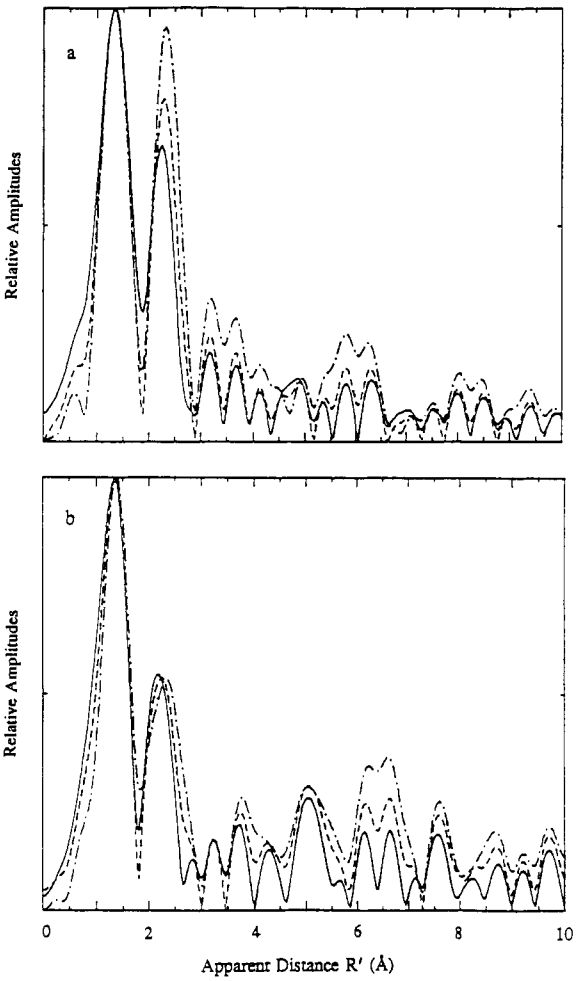

FIGURE 7: Fourier transforms of (a) the EXAFS of an S_2 state PSII preparation and (b) the difference EXAFS of an S_3 state preparation, prepared by the ferricyanide procedure. The apparent distance R' is shorter than the actual distance to a given neighboring atom due to the effect of the averaged phase, $\langle d\alpha(k)/dk\rangle_k$, of the EXAFS wave. The three Fourier transforms shown in (a) and (b) were obtained by multiplying the data by k (—) the photoelectron wave vector amplitude, k^2 (---), and k^3 (-·-).

The intensity of this feature has been shown to be a function of the symmetry of the metal complex (Shulman et al., 1976). The inset in Figure 5 is an expanded view of this transition. The intensity and shape of this feature in the S_3 spectrum are similar to the 1s → 3d transitions we recently reported for the S_2 state (Sauer et al., 1988).

X-ray Absorption Fine Structure Analysis. EXAFS spectra for PSII preparations poised predominantly in the S_3 state using the ferricyanide procedure and for S_2 state preparations were recorded. A "thermally relaxed" S_3 sample prepared by warming a sample prepared by the PPBQ method to 293 K in the dark for 30 s was also examined. EXAFS of the S_3 state preparations were analyzed by difference spectroscopy. A fraction of the EXAFS of a control S_2 state preparation was subtracted from the EXAFS of the S_3 state preparations that contained a residual S_2 state composition indicated by the multiline signal amplitude (see Tables I and II). Figure 6 contains the EXAFS spectrum of a PSII preparation poised in the S_2 state and the difference EXAFS spectrum of a PSII preparation poised in the S_3 state by illumination at 240 K following the ferricyanide procedure. The solid line in Figure 6 is the Fourier isolate of the two peaks evident in the Fourier transforms of the k_3-weighted EXAFS spectrum shown in Figure 7.

Two major peaks are evident in the Fourier transforms of the EXAFS spectra in both the S_2 and S_3 preparations (Figure 7). These peaks represent maxima in the backscattering of outgoing photoelectron waves and appear as a function of the distance between the central absorbing atom and neighboring atoms. The apparent distance (R') to a given scattering shell is shorter than the internuclear distance between the central absorbing atom and the ligating atoms owing to a contribution of the effect of an average phase shift [$\langle d\alpha(k)/dk\rangle_k$]. The phase shift [$\alpha(k)$] is induced by the effect of the potentials of the metal absorber and its ligands on the photoelectron.

k-Weighting Behavior. By multiplying EXAFS spectra by increasing powers of k (the photoelectron wave vector amplitude), EXAFS waves whose envelopes peak at higher k values are preferentially enhanced. These waves are due to backscattering from heavier elements. Thus, the Fourier transforms of peaks containing contributions from heavier elements increase more with k weighting than do peaks associated with scattering from light elements. This k-weighting behavior has been used previously to determine whether a transition metal is present in a given shell, as seen in the transform of the EXAFS of a metalloenzyme (Kirby et al., 1981; Woolery et al., 1984; Yachandra et al., 1986). In the Fourier transforms of the EXAFS of the S_2 preparation, the second peak increases in a manner consistent with significant contributions from heavy scatterers, such as a neighboring transition metal in a multinuclear cluster (see Figure 7). The details of the k-weighting behavior of the Fourier transform

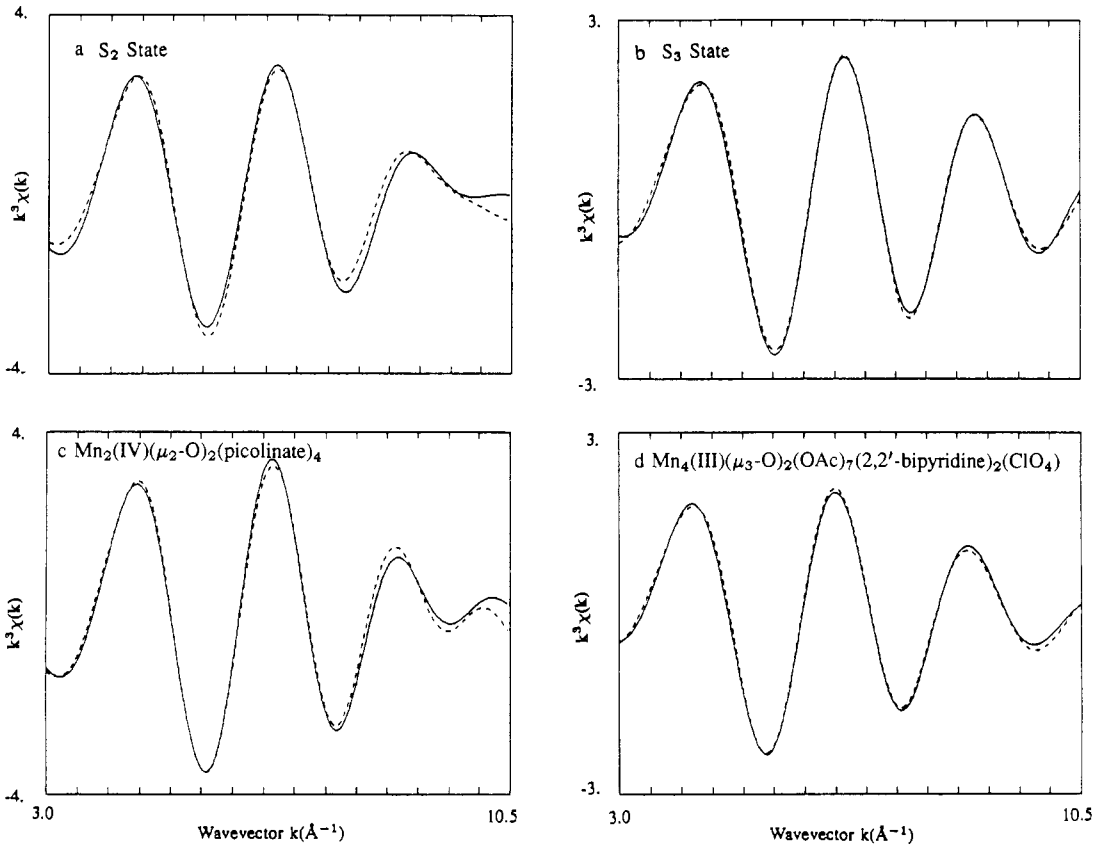

FIGURE 8: The lowest frequency component, or first shell, of the Mn EXAFS of PSII preparations poised in the S_2 and S_3 states. This low-frequency component is obtained by multiplying the Fourier transformed data by a function that isolates the peak in the Fourier transform occurring at the shortest effective distance. This spectrum is then back-transformed and simulated by using theoretically calculated amplitude and phase functions. The best fits to the "Fourier-isolated" first shell spectra are indicated by the dashed traces. The simulations shown are best fits assuming two different Mn–O distances. The spectra shown are of (a) the EXAFS of an S_2 state preparation, (b) the difference EXAFS of an S_3 state preparation, (c) a dimeric di-μ-oxo-bridged Mn complex (complex **2**) ligated by a mixture of carboxylates and heterocyclic rings, and (d) a tetranuclear manganese complex (complex **4**) with four inequivalent manganese centers. Simulation parameters for the fits shown are contained in Tables III and IV.

Table III: Simulation Results for the First Coordination Sphere of PSII Preparations Poised in the S_2 and S_3 States; k^3-Weighted EXAFS Data

	Mn–O (bridging ligands)				Mn–O or –N (terminal ligation)				
state	N	R (Å)	σ^2 (Å^2)	ΔE_0	N	R (Å)	σ^2 (Å^2)	ΔE_0	F^c
S_2[a]	1.8	1.77	0.007	−13	2.8	2.23	0.013	−20	9.73
S_3[b]	1.8	1.81	0.009	−11	2.1	2.20	0.015	−20	1.21

[a] Average results obtained from the simulation of the EXAFS of PSII preparations poised in the S_2 state. In general, distances obtained for individual samples differed by less than 0.02 Å. The number of scatterers determined at a given distance was found to be within 30%. [b] Difference EXAFS of a PSII preparation poised in the S_3 state by the ferricyanide procedure. This sample was illuminated at 240 K. Difference EXAFS results obtained for a S_3 state PSII sample prepared by the PPBQ procedure were in good agreement with the results presented for samples prepared by the ferricyanide method. [c] F is the least-squares difference between the Fourier-isolated EXAFS and the EXAFS calculated by using theoretically derived phase and amplitude functions (Teo & Lee, 1979).

peaks in these two states would appear to differ substantially. As is described below, this is probably due to differences in the static disorder in the Mn–Mn distances present in each state.

Simulations of the First Shell Indicate a Di-μ-oxo-Bridged Structure. The best fits to the Fourier isolates of the first shell of the EXAFS of an S_2 state PSII preparation and that of the difference EXAFS of an S_3 state preparation are shown in Figure 8, panels a and b, respectively. In both cases, simulations including two O or N waves were found to be significantly better than single-wave fits. The difference between the two distances obtained in the two-wave fits is consistent with the proposition that the static disorder present in the EXAFS waves, which yields this broad peak in the transforms of Figure 7, is larger than can be adequately described with a single Debye–Waller factor (Brown & Eisenberger, 1979). Simulation results for the first shell of the EXAFS of the S_2 state preparations and the difference EXAFS of the S_3 state preparations are contained in Table III.

In addition to the quality of the fits obtained, the parameters obtained for the two unresolved shells are eminently reasonable in light of what is known about the bonding in multinuclear oxo-bridged manganese complexes. The simulation yields a short Mn–O or Mn–N bond that displays a relatively small degree of disorder and a set of longer bonds spread over a greater range of distances. These two sets of first shell ligands correspond remarkably well to the bridging and terminal ligands observed in multinuclear oxo-bridged manganese complexes (Plaksin et al., 1972; Wieghardt & Bossek, 1983; Sheats et al., 1987; Vincent et al., 1987).

The shorter Mn–O distance to the "bridging" shell is on the average ~0.04 Å longer in the S_3 preparations than in the S_2 preparations. Although this systematic difference appears to be real, care must be exercised in attempting to assign the nature of this change to a specific structural rearrangement. The uncertainties in the distances obtained from the simulation

Table IV: Simulation Results for the First Coordination Sphere of Four Site Models;[a] k^3-Weighted EXAFS Data

	Mn–O (bridging ligands)				Mn–O or –N (terminal ligation)				
model no.	N	R (Å)	σ^2 (Å^2)[c]	ΔE_0	N	R (Å)	σ^2 (Å^2)	ΔE_0	F[d]
1	1.7 (2.0)	1.75 (1.82)	0.005 (0.0016)	−10	3.7 (4.0)	1.95 (2.11)	0.023 (0.006)	−20	13.5
2	1.5 (2.0)	1.79 (1.82)	0.005 (0.000)	−10	2.8 (4.0)	2.23 (1.97)	0.006 (0.010)	−20	6.0
3	2.1 (3.0)	1.74 (1.78)	0.005 (0.0005)	−10	3.7 (3.0)	2.03 (2.09)	0.010 (0.006)	−20	27.8
4	1.4 (1.5)	1.83 (1.88)	0.010 (0.0025)	−10	2.0 (4.5)	2.23 (2.07)	0.028 (0.014)	−20	0.4

[a] The site models examined here are $Mn^{III}Mn^{IV}(\mu_2\text{-}O)_2(bipy)_4(ClO_4)_3$ (**1**), $Mn^{IV}_2(\mu_2\text{-}O)_2(picolinate)_4$ (**2**), $Mn^{IV}_4(\mu_2\text{-}O)_6(tacn)_4(ClO_4)_4$ (**3**), and $Mn^{III}_4(\mu_3\text{-}O)_2(OAc)_7(bipy)_2(ClO_4)$ (**4**). [b] Numbers in parentheses are EXAFS simulation parameters calculated from the crystal structure of each inorganic complex. Only the static contribution to the Debye–Waller has been calculated here. Since the thermal contribution is often as large or larger than the static term, the simulated values are invariably larger than the calculated static values. [c] For the μ-oxo shell the Mn–O Debye–Waller term was constrained to reasonable values, except for complex **4** for which a very well-defined minimum was obtained at the indicated value. [d] F is the least-squares residual difference between the Fourier-isolated EXAFS and the EXAFS calculated by using theoretically derived phase and amplitude functions.

of two unresolved components are often higher (e.g., ±0.05 Å) due to the correlation between the amplitude of one component and the mean distance to the other unresolved scattering shell (Brown & Eisenberger, 1979).

To refine the simulation parameters obtained from the Mn EXAFS of the PSII preparations, four structurally characterized multinuclear manganese compounds were examined in detail and their EXAFS simulation parameters compared to that of the PSII preparations poised in the S_2 and S_3 states. Three of these four inorganic complexes, $Mn^{III}Mn^{IV}(\mu_2\text{-}O)_2$-(2,2′-bipyridine)$_4(ClO_4)_3$ (**1**) (Plaksin et al., 1972), Mn^{IV}_4-$(\mu_2\text{-}O)_6(tacn)_4(ClO_4)_4$ (**3**) Wieghardt & Bossek, 1983), and $Mn^{III}_4(\mu_3\text{-}O)_2(OAc)_7$(2,2′-bipyridine)$_2(ClO_4)$ (**4**) (Vincent et al., 1987), have been proposed as site models for the manganese cluster within the OEC of PSII (Kirby et al., 1981; Brudvig & Crabtree, 1986; Vincent et al., 1987). The similarity of the 16-line EPR spectrum exhibited by complex **1** to the multiline EPR spectrum exhibited by PSII membrane suspension poised in the S_2 state was the first evidence implicating a functional role for Mn in photosynthetic O_2 evolution (Dismukes & Siderer, 1981). Also, Mn–Mn and Mn–O distances obtained by simulation of the EXAFS of the Mn complex in PSII are similar to distances obtained from the simulation of the EXAFS of **1** (Kirby et al., 1981; Yachandra et al., 1986, 1987). Complex **2** is structurally similar to **1**; however, unlike **1** the terminal ligation is a mixture of carboxylates and heterocyclic rings. Complex **3** is a tetranuclear Mn(IV) adamantane-like structure which has been proposed to be a model for the Mn complex of PSII poised in the S_3 state (Brudvig & Crabtree, 1986). Complex **4** is a tetranuclear Mn(III) complex which consists essentially of a di-μ-oxo-bridged core structure with two additional Mn atoms mono-μ-oxo bridged to the dimeric core via three-centered oxygen bridges. Complex **4** is unique among the complexes examined in this study in that it contains two different Mn–Mn distances. Like complex **2**, this complex has a heterogeneous terminal ligation containing both carboxylates and heterocyclic rings.

The static Debye–Waller factor, the mean distance to each scattering shell, and the number of scatterers in each shell were calculated for each model by using the crystallographic coordinates (see numbers in parentheses in Table IV). The magnitude of the thermal contribution to the Debye–Waller factor can be estimated from measured symmetric stretching frequencies in the IR (Teo, 1986). For strong bonds, this thermal contribution to the Debye–Waller factor in angstroms is approximated by

$$\sigma = 4.106(1/\mu\nu)^{1/2}$$

where ν is the vibrational frequency in cm^{-1} and μ is the reduced mass in daltons.

On the basis of ^{18}O substitution studies of the bipyridine binuclear complex (complex **1**), the 688-cm^{-1} band in the IR was assigned to the Mn–O bridging mode (Cooper & Calvin, 1977). From this value, the magnitude of the vibrational contribution to the Debye–Waller factor is estimated to be σ^2 = 0.0020 Å^2.

The correlation between unresolved components was more of a problem for most of the inorganic compounds than for the PSII preparations. Unconstrained Debye–Waller factors for the μ-oxo bridging shell approached zero for all inorganic complexes except **4**. To decrease this effect in the model complex simulations, a reasonable value containing approximately equal static and dynamic contributions was assumed (e.g., 0.005 Å^2). The best fit parameters for the simulation of the first shell of each model complex are contained in Table IV.

Refinement of the simulations of the first coordination sphere of the PSII EXAFS based on the EXAFS of structurally related inorganic compounds indicates that the manganese present in PSII is principally in the form of binuclear units. Thus the four manganese atoms present in PSII could be organized as a pair of di-μ-oxo-bridged binuclear clusters or possibly a trinuclear manganese cluster containing di-μ-oxo bridges between manganese atoms and an isolated Mn center. Both of these configurations would yield an average of two bridging oxygens seen by each Mn atom within PSII. A trinuclear structure associated with an isolated mononuclear structure has recently been proposed as a possible structure for the four manganese atoms present in the oxygen-evolving complex (Li et al., 1988) on the basis of trinuclear complexes that have been synthesized and the suggestion that the g = 4.1 EPR signal associated with the S_2 state may be due to a mononuclear Mn(IV) center (Hansson et al., 1986). It should be noted, however, that to date no inorganic trinuclear complexes have been synthesized with Mn–Mn distances resembling those observed in the manganese complex in PSII.

For the S_2 state the simulation results (Table III) are remarkably similar to those of complex **2** (Table IV). This is revealed not only by the similarity of the parameters obtained through simulation but also by the striking similarity of the EXAFS waves of complex **2** and the Mn complex in PSII poised in the S_2 state (see Figure 8a,c). Further, the variation in the apparent number of scatterers in the first shell obtained by systematically varying the Debye–Waller factor most closely resembles the variation observed in the PSII preparations poised in the S_2 state (Guiles, 1988). These criteria have been suggested by Teo et al. (1983) for the selection of a model for use in determining a scale factor (e.g., the number of scatterers determined by simulation divided by the number calculated on the basis of the crystal structure) to refine the number of atoms in a given scattering shell. Applying the scale factor obtained from complex **2** to the number of μ-oxo bridges determined for the Mn complex in the OEC, one obtains 2.4

Table V: Simulation Results for the Second Shell of PSII Preparations Poised in the S_2 and S_3 States; k^3-Weighted EXAFS Data

	Mn–Mn				Mn–C				
state	N	R (Å)	σ^2 (Å^2)	ΔE_0	N	R (Å)	σ^2 (Å^2)	ΔE_0	F
S_2[a]	1.2	2.72	0.005	−10	3.4	3.13	0.010	−12	5.6
S_3[b]	1.2	2.72	0.014	−10	2.0	3.15	0.010	−17	8.2

[a] Average results obtained from the simulation of the EXAFS of PSII preparations poised in the S_2 state. In general, distances obtained for individual samples differed by less than 0.02 Å. The number of scatterers determined at a given distance was found to be within 30%. [b] Difference EXAFS of a PSII preparation poised in the S_3 state by the ferricyanide procedure. This sample was illuminated at 240 K. Difference EXAFS results obtained for an S_3 state PSII sample prepared by the PPBQ procedure were in good agreement with the results presented for samples prepared by the ferricyanide method.

oxygens per Mn. Note that this result is inconsistent with the four Mn atoms present in PSII being organized as a binuclear di-μ-oxo-bridged manganese complex and two associated mononuclear manganese centers, which would yield an average number of one μ-oxo bridging oxygen seen by each Mn.

The EXAFS due to the first coordination sphere of complex **4** are nearly superimposable on those of the Mn complex in PSII poised in the S_3 state (see Figure 8b,d). Also, the simulation results assuming two oxygen waves for the first coordination sphere of the manganese complex in PSII in the S_3 state most closely resemble those of complex **4**. Unlike that of complex **4**, the simulation of the EXAFS of the first shell for the other inorganic complexes improves substantially upon addition of a third O or N wave, which suggests that the complex envelope of the EXAFS of the first shell of these complexes is inadequately modeled by two light-element waves. This does not mean that complex **4** is the best site model for the manganese cluster in the OEC in the S_3 state; in fact, simulations of the second shell which indicate two distinct Mn–Mn distances (see simulations of the second shell below) rule this complex out as a reasonable site model. However, as described above, the strikingly similar parameter correlations exhibited in simulations of the first shell permit a more accurate determination of the number of scatterers in the first coordination sphere. For the μ-oxo bridging shell, a scale factor (see Materials and Methods) of 1.07 is obtained. For the first shell EXAFS of the S_3 state preparation this yields a value of 1.9 ± 1.0 bridging oxygens seen by each Mn present in PSII. This result taken together with the results for the S_2 state suggests a di-μ-oxo-bridged structure. This average number of bridging oxygens is inconsistent with a higher nuclearity complex such as an adamantane-like complex (e.g., complex **3**) or a symmetric cubane tetranuclear cluster, both of which possess three μ-oxo bridges to each manganese atom.

Simulations of the Second Shell. The assignment of a manganese scatterer to the peak at higher apparent distance in the Fourier transform of the EXAFS of the PSII samples is reasonable from several lines of evidence. The k-weighting behavior of this transform peak is indicative of a heavy scatterer such as manganese, although EXAFS is not capable of discriminating between adjacent elements such as Mn and Fe (Kirby et al., 1981; Yachandra et al., 1986). The similarity of the EPR of the S_2 state (the multiline signal) to that of binuclear manganese model complexes strongly suggests the assignment of a manganese neighbor (Cooper et al., 1978). Also, the distance obtained (2.72 Å), if a single manganese neighbor is assumed, is consistent with the distances known in di-μ-oxo-bridged binuclear manganese complexes (Plaksin et al., 1972; Stebler et al., 1986).

Fits to the second shell indicate that a single wave (in this case, a manganese scatterer) is inadequate to describe the disordered shell. Unlike the first shell, the origin of the heterogeneity in the second shell is less clearly defined. On the basis of an examination of the crystallographic data of a variety of manganese models containing biomimetic ligands (e.g., carboxylates, phenoxy complexes, or heterocyclic ring structures) it is clear that the second shell must contain some light elements (probably carbon; see Table VI). Considering the generally accepted stoichiometry of four manganese per PSII reaction center, the heterogeneity observed in the second shell could be due to static disorder in the Mn–Mn distance, for example, due to variation in the separation between manganese neighbors within two isolated binuclear complexes.

Unconstrained fits to the second shell EXAFS of PSII preparations poised in the S_2 state assuming a Mn shell and a shell of light scatterers (carbon atoms) yield a Mn–Mn Debye–Waller factor of 0.0078 Å^2 and an average number of Mn neighbors equal to 1.4 ± 0.4. However, the value of the Debye–Waller factor obtained for the presumably highly disordered Mn–C shell approached zero. This counterintuitive simulation result has been observed before in highly disordered systems exhibiting unresolved EXAFS shells (Eisenberger & Lengeler, 1980). The effects of shell correlation can limit the accuracy in the determination of the number of scatters to ±50%. To limit these effects, the Debye–Waller factor for both the Mn–Mn shell and the Mn–C shell were constrained to reasonable values (e.g., σ_{Mn-Mn} = 0.005 Å^2 and σ_{Mn-C} = 0.010 Å^2). The dominant contribution of the Debye–Waller factor for the Mn–Mn shell is the thermal term. By use of these constraints 1.2 Mn neighbors are observed for the Mn complex in PSII preparations poised in the S_2 state.

Table V contains a summary of the simulation results for the second shell of EXAFS of the Mn complex in the PSII preparations. On the basis of the analysis of model complexes we have found that inclusion of a shell of light atoms greatly improves the accuracy in the determination of the number of Mn atoms present (Guiles, 1988). Figure 9 contains the best fits to the second shell assuming a Mn neighbor and a carbon shell.

The dominant consequence of the high disorder of the light atoms (carbons) present in the second shell in all the inorganic complexes is a mutual annihilation of EXAFS waves. One positive effect is that the scattering of transition metal neighbors tends to dominate the scattering characteristics of the outer shell, partially because of a lower disorder and partially due to the larger intrinsic backscattering power. The result is that simulation of the outer shell yields very accurate estimates of the distance to these dominant scatterers. For example, simulations of complexes **1** and **2** yield values that are within 0.03 Å of the crystallographic values (see Table VI). It is also interesting to note that complex **4** exhibits two distinct Mn–Mn distances that differ by nearly 0.5 Å. Simulations of the second shell assuming one Mn–Mn distance and a shell of carbon atoms are totally inadequate to describe the complex beat pattern exhibited in the second shell of this model. As is evident from the simulation results, the distances to the neighboring Mn atoms in this complex are also accurately determined (again to within ±0.03 Å).

Fits to the second shell of the Mn EXAFS of PSII preparations poised in the S_3 state using the constraints on the

Table VI: Simulation Results for the Second Shell of Four Site Models; k^3-Weighted EXAFS Data

	Mn-Mn				Mn-C				
model no.	N	R (Å)	σ^2 (Å^2)[b]	ΔE_0	N	R (Å)	σ^2 (Å^2)	ΔE_0	F
1	0.8 (1.0)	2.72 (2.72)	0.005 (0.000)	−1	1.4 (8.0)	3.07 (3.02)	0.010 (0.0092)	0.0	24.4
2	1.0 (1.0)	2.72 (2.75)	0.005 (0.000)	−10	1.1 (6.0)	2.88 (2.89)	0.010 (0.0015)	−2	9.0
3	1.5 (3.0)[c]	3.25 (3.22)	0.005 (<0.001)	0	3.2 (6.0)	2.90 (2.94)	0.010 (0.0026)	−1	70.3
	Mn-Mn				Mn-Mn[d]				
model no.	N	R (Å)	σ^2 (Å^2)[b]	ΔE_0	N	R (Å)	σ^2 (Å^2)	ΔE_0	F
4	0.6 (0.5)	2.87 (2.85)	0.005 (0.000)	−4	0.5 (2.0)	3.34 (3.34)	0.005 (0.0018)	−9	0.4

[a] Numbers in parentheses are EXAFS simulation parameters calculated from the crystal structure of each inorganic complex. Only the static contribution to the Debye–Waller has been calculated here. Since the thermal contribution is often as large as or larger than the static term, the simulated values are invariably larger than the calculated static values. [b] The Debye–Waller term for the Mn–Mn shell was constrained to reasonable values. [c] The low number of manganese neighbors predicted by simulation of the EXAFS of this model is principally a consequence of the fact that two waves (i.e., a Mn–Mn and Mn–C wave) are inadequate to describe the second shell EXAFS of this inorganic complex. A well-defined shell of oxygens at 3.44 Å also exists in this complex. Inclusion of a third oxygen wave improves the fit quality substantially (e.g., $F = 46$) and yields a much better estimate of the number of manganese neighbors (e.g., 2.4). [d] Complex **4** has two Mn–Mn distances which differ by more than 0.5 Å. Simulations of this complex assuming a single Mn neighbor are inadequate to describe the complex beat structure exhibited by the EXAFS of this complex.

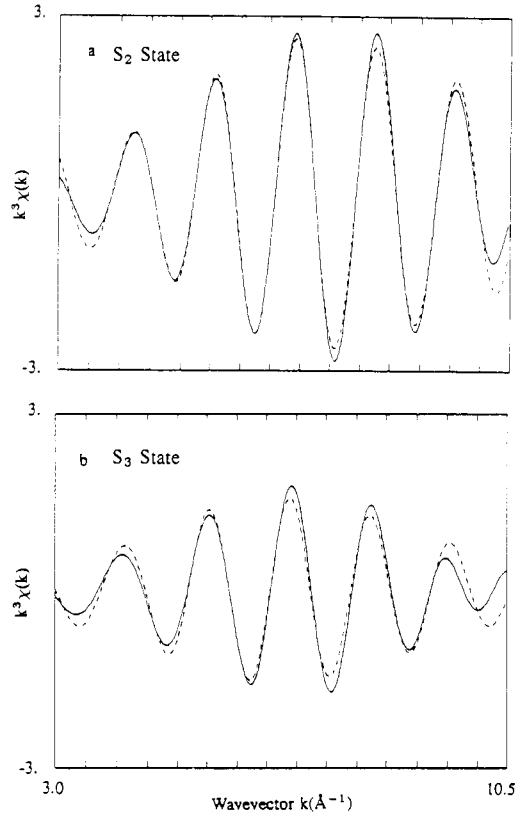

FIGURE 9: Fourier components (—) of the k^3-weighted EXAFS of PSII preparations corresponding to the peak at longer distance in the Fourier transforms shown in Figure 7. Best fits to this outer scattering shell are also plotted (---). The curves plotted in (a) are the second shell spectra and fits of a PSII preparation poised in the S_2 state. The curves plotted in (b) are the second shell difference EXAFS spectra and fits of an S_3 state preparation. The simulations plotted are two-component simulations assuming a Mn–Mn wave and a Mn–C EXAFS wave. The results of these simulations are contained in Table VI.

Debye–Waller factors described above yield a smaller number of manganese neighbors (e.g., 0.6 Mn). It is important to note that the fit quality obtained with these constraints is substantially poorer. The least-squares residual was 21, compared to 5.6 for the S_2 state prepartion. Both the envelope shape and reduced amplitude of the the EXAFS waves due to second shell scatterers in samples poised in the S_3 state (see Figure 9) are indicative of a higher degree of disorder than is observed in the corresponding shell in the S_2 state preparations. If the Debye–Waller factor for the Mn–Mn shell is allowed to float, substantially better fits are obtained, yielding larger values for the Mn–Mn Debye–Waller factor. Simulations of the S_3 state second shell EXAFS of nearly equal quality to those obtained for the S_2 state preparation are obtained when the number of apparent scatterers is the same as that obtained for the S_2 state preparations (see Table V).

Given that backscattering from the manganese tends to dominate, most probably the increase in disorder shown by the fits to the PSII Mn EXAFS upon advancing to the S_3 state is due to an increase in the spread of Mn–Mn distances. This indicates the presence of two inequivalent binuclear complexes in the S_3 state or distortions in a higher nuclearity complex. Simulations including two inequivalent manganese neighbors for the manganese center of PSII indicate that if a heterogeneity in the Mn–Mn distance exists, then the spread in this distance is approximately 0.15 Å. The same conclusion can be drawn from the value of the Debye–Waller factor when a single Mn neighbor is assumed (e.g., the spread indicated by the Debye–Waller factors is 0.09 Å for the S_2 state and 0.13 Å for the S_3 state). This indicates that the disorder observed in the second shell of the PSII preparations is due to variation in the Mn–Mn distance.

Of the four inorganic model complexes, **2** matches the simulation properties of the second shell of the manganese complex in PSII most closely. As was the case with the first coordination sphere, the second shell EXAFS of complex **2** bears a striking similarity to that of the Mn complex in PSII. In the simulations of both **2** and the manganese center in PSII, a short Mn–Mn distance (2.7 Å) and a shell of carbon atoms near 3 Å are obtained. When the scale factor obtained from **2** is applied, 1.2 ± 0.5 Mn neighbors are obtained for the manganese cluster in PSII in the S_2 state and 1.2 ± 0.7 Mn neighbors for the S_3 state. A single manganese dimer and two monomeric manganese sites would yield an average number of manganese neighbors equal to 0.5 per Mn, which is inconsistent with the lower limit of the observed values of this range for the S_2 state and at the lower limit of the range of the S_3 state. Taken together with the results from the first coordination sphere and given the stoichiometry of four Mn per PSII reaction center, this implies the presence of two binuclear manganese structures or a mononuclear center and a trinuclear complex.[3]

[3] A linear trinuclear complex with the Mn atoms separated by ~2.7 Å is unlikely because one would expect an intense Fourier peak at ~5 Å due to the focusing effect of the middle manganese atom. However, a bent trinuclear complex cannot be ruled out.

The magnitudes of Fourier peaks associated with Mn shells in the region around 3.2 Å in the EXAFS of compounds **3** and **4** are substantially greater than features present in this region in the Fourier transform of the EXAFS of the PSII preparations. This indicates that discrete tetranuclear complexes such as compounds **3** and **4** are not reasonable models for the Mn site in PSII. Symmetric tetranuclear cubane-like complexes would be expected to yield an average number of Mn neighbors equal to three, which is also inconsistent with the number determined for the Mn complex in PSII.

Recently, George et al. (1989) published results indicating a Mn–Mn neighbor at 3.3 Å on the basis of EXAFS analyses of oriented chloroplast membranes. Previously, in a preliminary report (Guiles et al., 1987), we have reported a feature at $R > 3$ Å as possible evidence of scattering by a transition metal. This result was obtained from data generated by adding EXAFS data from a PSII sample in the S_1 state to those of one in the S_2 state in an attempt to increase the signal-to-noise ratio. We have not reproduced this observation with our current detection method. Thus we cannot state that we observe features in the current data sets which confirm the report of George et al. Since George et al. (1989) do not report unoriented spectra, it is difficult to directly compare their results with ours. Nonetheless, we do not see features of a magnitude consistent with their observation in the region around 3.3 Å. We also do not see any evidence of a significant feature at 3.8 Å for which George et al. do not offer detailed explanations. It is important to note that the data of George et al. were recorded at a different temperature (4 K) and have a higher signal-to-noise ratio than the data presented in this article. This higher data quality has enabled them to analyze their data out to higher k values than we have been able to do at the present time. This may in part explain some of the differences observed.

It is important to note that while Fourier isolation of individual scattering shells can greatly facilitate convergence of the nonlinear least-squares minimization used in fitting the EXAFS, Fourier isolation also introduces distortions. Window functions often remove Fourier components of the EXAFS waves potentially important in defining the envelope shape and phase behavior. Simulating a Fourier isolate of a broader range of frequency components (e.g., including at least the two peaks in the Fourier transform shown in Figure 7) substantially reduces these distortions. Simulations of the EXAFS of the Mn complex in PSII poised in the S_2 and S_3 states performed on a Fourier isolate of both scattering shells largely confirm the results obtained by simulation of individual shells. Figure 10 contains the Fourier isolate of the first two shells together with a three-component fit including one Mn–Mn wave and two Mn–O waves. Simulation results are indicated in the figure caption.

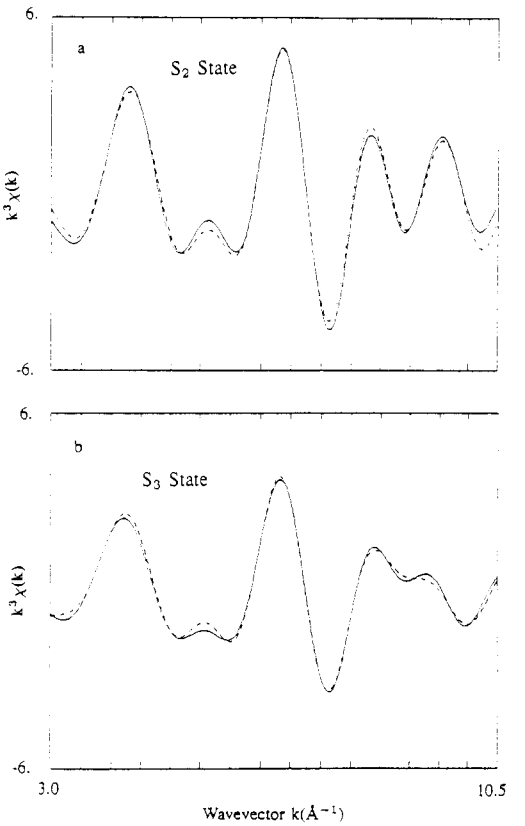

FIGURE 10: Fourier components (—) of the k^3-weighted EXAFS of PSII preparations corresponding to both peaks at in the Fourier transforms shown in Figure 7. Best fits to these scattering shells are also plotted (---). The curves plotted in (a) are the spectra and fits of a PSII preparation poised in the S_2 state. The curves plotted in (b) are the difference EXAFS spectra and fits of an S_3 state preparation. The simulations plotted are four-component simulations assuming a Mn–Mn wave and a Mn–C and two Mn–O EXAFS waves. Results obtained for the two fits are as follows. For the S_2 state preparation EXAFS shown, simulations yielded 1.2 Mn neighbors at 2.76 Å, 3.4 carbons at 3.13 Å, 1.4 oxygen ligands at 1.78 Å, and 2.0 oxygens ligands at 2.22 Å. Debye–Waller factors for these three shells were 0.005, 0.010, 0.004, and 0.003 Å^2, respectively. For the S_3 state EXAFS, simulations yielded 1.2 Mn at 2.76 Å, 2.0 carbons at 3.15 Å, 1.6 oxygens at 1.81 Å, and 1.6 oxygens at 2.19 Å. Debye–Waller factors for these four shells are 0.013, 0.010, 0.010, and 0.006 Å^2, respectively. These results are in good agreement with results obtained from the simulation of individual scattering shells. Note that the constraints which were used in the simulation of the individual shells were also applied here.

Discussion

Factors Limiting Complete S_3 State Conversion. Of the two procedures used to prepare PSII membrane preparations poised in the S_3 state, that involving ferricyanide oxidation yielded a significantly lower S_2 state residual. This difference is principally due to the elimination of the competitive photooxidation of cyt b_{559} that occurred in the PPBQ experiments. Previous EPR studies of PSII membranes (de Paula et al., 1985) have shown that cytochrome b_{559} is the principal electron donor at 77 K. These authors showed that only 0.9 ± 0.1 cytochrome of the 2 cytochromes present in PSII is photooxidized at 77 K. However, they found that 2.1 ± 0.2 cytochromes could be oxidized in the dark using ferricyanide. Thus, the 77 K illumination used in the oxidation of Q_{400}, using PPBQ, resulted in the oxidation of only about half of the available high-potential cyt b_{559}. The remaining reduced cyt b_{559} was found to be a significant competitive donor in the second low-temperature illumination used to generate the S_3 state. These results confirm similar observations made by Styring and Rutherford (1988) concerning the temperature dependence of of the S_2 to S_3 state transition and provide a plausible explanation for the incomplete turnover. The PPBQ procedure used to generate the S_3 state did have one significant advantage over the ferricyanide procedure; the charge-separated state attained following the double-turnover illumination procedure was found to be significantly more stable than that achieved in the ferricyanide experiments.

The incomplete double turnover of PSII observed in the experiments using ferricyanide to generate Q_{400} is probably due to the presence of reaction centers in which Q_{400} is not functional. Ikegami and Katoh (1973) observed fluorescence induction behavior corresponding to as much as a full additional acceptor equivalent in chloroplasts following ferricyanide oxidation and DCMU treatment. However, Petrouleas and

Diner (1987) have found through an analysis of the decay kinetics of the C-550 band associated with pheophytin that the reoxidation of $Q_A^-Fe^{2+}$ exhibits biphasic kinetics. A fast 25-μs component was attributed to reoxidation by Q_{400} while a slower (100-μs) component was attributed to electron transfer from Q_A^- to Q_B. Quantitation of the amplitude of each of these components led Petrouleas and Diner (1987) to suggest that as little as 50% of the reaction centers contained oxidized acceptor–iron complexes. Thus, incomplete oxidation of Q_{400} may have been a limitation in observing a complete double turnover in all reaction centers. Alternatively, de Paula et al. (1985) have observed competitive donation of a radical species at low temperatures in preparations in which both cytochrome b_{559} centers had been chemically oxidized. Although a chlorophyll or carotenoid radical has not been observed at the temperatures of illumination used in the ferricyanide experiments, it is suggested that competitive donation by a chlorophyll or a carotenoid species may have contributed to the decreased yield of the S_3 state.

X-ray Absorption Edges. Manganese does not appear to become more oxidized during the $S_2 \rightarrow S_3$ transition. The average inflections of the Mn X-ray absorption edges of the three different S_3 state preparations were found to be within 0.2 eV of the edge energy of the S_2 state preparations. The invariance in the energy of the edge and the shape of the edge indicate that the manganese cluster remains at the same oxidation state during the $S_2 \rightarrow S_3$ state transition. Significant changes in the structure of the 1s $\rightarrow$ 3d transition of the Mn K-edge of PSII preparations are observed during the $S_1 \rightarrow S_2$ state transition (Sauer et al., 1988). These changes indicate a valence change from Mn(III) to Mn(IV). The similarity of the preedge structure of the S_3 state (see inset of Figure 5) to the structure that we have previously reported for the S_2 state (Sauer et al., 1988) implies that the oxidation state and site symmetry are unchanged during the $S_2 \rightarrow S_3$ state transition. It might be argued that an increase in the valence of the manganese complex of PSII preparations poised in the S_3 state relative to that of the S_2 state might not be indicated by the expected increase in the energy of the Mn K-edge, owing to a coincidentally equal decrease in edge energy induced by a change in the site symmetry of the Mn complex occurring during the $S_2 \rightarrow S_3$ transition. However, it is highly unlikely that both the Mn K-edge energy and all other spectral features of the Mn K-edge would remain the same after both an oxidation state change and a significant change in the symmetry of the complex.

This absence of change in the K-edge energy and structure indicates that the oxidative equivalent stabilized on the donor side of PSII during the S_2 to S_3 transition is stored on a redox-active center other than Mn. This result is surprising in light of the loss of the multiline EPR signal associated with the manganese complex in the S_2 state and suggests that the oxidative equivalent stabilized on the donor side of PSII is located on another intermediate donor very close to the manganese complex. We speculate that strong exchange coupling between an oxidized intermediate and the manganese complex results in a spin system with zero net spin or in an EPR-silent non-Kramers state.[4] The rapid decrease in the magnitude of exchange coupling as a function of the distance between paramagnetic centers (Coffman & Buettner, 1979) indicates that this putative paramagnetic intermediate is directly ligated to the manganese complex or very near (<7 Å, assuming a strong exchange coupling in the range of $J \sim 100$ cm^{-1}). Alternatively, strong dipolar coupling between this putative paramagnetic intermediate and the Mn species yielding the multiline signal could alter the relaxation properties of the complex, resulting in an EPR signal that is too broad to be observed. The small change in the manganese structure between the S_2 and S_3 states indicated by the EXAFS analyses is suggestive of a change in a species coordinated to the manganese complex. Aromatic species that are potential candidates for this putative intermediate are quinones (Goodin et al., 1984), tyrosines, histidines, or tryptophans (Sivaraja et al., 1989). Tyrosines have recently been associated with the intermediate Z (Debus et al., 1988a,b). While partial oxidation of the substrate water might also explain the lack of change in the manganese oxidation state, a thermodynamic analysis of water oxidation chemistry indicates that this is unlikely (Krishtalik, 1986). It is of note that the current estimate of the number of quinones in PSII preparations is two per reaction center (Takahashi & Satoh, 1987). Since one of these is presumably Q_A, the remaining one is a possible candidate for the intermediate suggested here.

The absence of changes in the oxidation state of the Mn in PSII during the $S_2 \rightarrow S_3$ transition is inconsistent with assertions made by Dekker et al. (1984) based on UV difference optical spectroscopy studies. However, an alternative interpretation of UV difference spectra put forth by Lavergne (1985) suggests that there may not be a change in the oxidation state of manganese during this transition. More recently, these interpretations have been revised (Lavergne, 1987). It should be noted that recently a consensus has been reached with regard to the nature and interpretation of specific absorption changes occurring during each S-state transition (Kretschmann et al., 1988). However, the assignment of specific oxidation state changes to the difference spectra observed in PSII can be difficult on the basis of optical difference spectra of structurally characterized multinuclear manganese complexes that could be prepared in more than one oxidation state (Vincent & Christou, 1986).

On the basis of studies of proton relaxation rates as a function of flash number, Srinivasan and Sharp (1986) have asserted that there is no oxidation of manganese occurring during the S_2 to S_3 transition. More recently, Rutherford and Styring (1987) measured the microwave power saturation of signal II_{slow} (D^+) in different S states and found a change in $P_{1/2}$ in the S_1 to S_2 transition, which they attributed to relaxation enhancement due to oxidation of Mn(III) to Mn(IV) in the O_2-evolving complex. No change was detected upon going from S_2 to S_3, which they suggest indicates that Mn is not oxidized during this transition. While one would expect that the spin-state change during the $S_2 \rightarrow S_3$ transition, which is indicated by the loss of the multiline signal, would alter the spin relaxation properties of D^+ or nearby protons, their conclusions are consistent with our interpretation of the Mn K-edge data.

EXAFS Analysis. Consistent with the lack of changes in the edge, relatively subtle structural changes are observed through analyses of the EXAFS of the manganese cluster in the S_2 and S_3 states. This is true for PSII preparations poised in the S_3 state by illumination at low temperature, as well as for samples that were "thermally relaxed" by warming to room temperature in the dark. The small increase in disorder observed is inconsistent with the major structural rearrangement

[4] Recently, an EPR signal associated with the S_3 state of Ca^{2+}-depleted PSII preparations has been observed (Boussac et al., 1989). Consistent with our proposal, this signal centered at around $g = 2$ and about 150 G wide has been attributed to an organic free radical interacting with the manganese complex. A similar signal has also been observed in our laboratory (M. J. Latimer, personal communication), and by Baumgarten et al. (1989).

from a cubane-like tetranuclear complex to an adamantane-like complex (complex **3**) that has been proposed to occur during this transition (Brudvig & Crabtree, 1986).

This small increase in disorder in the second shell observed for the S_3 state preparation is perhaps consistent with the apparent absence of enhancement of the second shell Fourier peak with increasing k weighting. Enhancement with k weighting for a scattering shell containing a heavy atom is not always observed. For example, Woolery et al. (1984) did not always observe enhancement of the second shell Fourier peaks in the EXAFS of hemocyanin (which contains a binuclear Cu complex with a Cu–Cu separation of 3.4–3.6 Å), depending on the state of the preparation (e.g., oxidized, reduced, or inhibitor bound). Similarly, the Fourier peak due to the second Mn shell at a mean distance of 3.34 Å in the open butterfly-like tetranuclear complex (complex **4**) is not enhanced with increasing k weighting (Guiles, 1988). Note that the spread of Mn–Mn distances in the second Mn shell of this complex is 0.07 Å. The lack of enhancement is presumably due to beat effects between two Mn waves with similar frequencies, which alters the shape of the envelope of the EXAFS wave.

Fine adjustments based on correction factors obtained from the inorganic complexes (complexes **2** and **4**) which mimic the EXAFS behavior of the manganese in PSII suggest that the four manganese present are in the form of two di-μ-oxo-bridged manganese binuclear complexes. Note that a structure consisting of a mononuclear center and a trinuclear complex is also consistent with the number of μ-oxo bridges and Mn neighbors determined from the EXAFS analysis. This conclusion is based on the remarkably similar parameter correlations of **2** with those of the Mn complex in PSII in both the first and second shells. However, the parameters obtained from the simulation of the EXAFS of the first coordination sphere of manganese in PSII in the S_3 state strongly resemble those of **4**. This open tetranuclear model (Complex **4**) is a more disordered structure than any of the other three models. All four manganese present are inequivalent (e.g., there are no crystallographically imposed symmetry constraints). The 18 different bond distances in the terminal ligation of this tetranuclear structure more closely approximate a continuous Gaussian distribution of distances, which apparently is adequately described by a single Gaussian Debye–Waller term. This may explain the significantly better fit obtained for the first coordination sphere of the manganese in the S_3 state using only two oxygen waves. Note, however, that the general agreement with the crystallographic distances for the terminal shell of complexes **4** and **2** is very poor. This is presumably due to the disorder present in the mixed O, N terminal coordination spheres in these complexes. Large absolute errors in the determination of distances to highly disordered shells have been described in other systems (Brown & Eisenberger, 1980). The striking similarity of the fit parameters for the first shell indicates that a di-μ-oxo-bridged structure with four inequivalent manganese centers is present in the OEC in the S_3 state. It is interesting to note that those inorganic complexes that exhibit EXAFS most similar to that of the Mn complex in PSII have heterogeneous ligation spheres containing both carboxylates and heterocyclic rings. On the basis of this observation, one may speculate that the manganese complex in PSII is ligated by a combination of carboxylates derived from acidic side chains and imidazole rings derived from histidine residues.

Conclusions

(1) The use of the high-potential acceptor Q_{400} in a double turnover of PSII produced by a single low-temperature illumination yields a PSII preparation with a substantial S_3 state composition.

(2) The energy of the Mn K-edge is the same for PSII preparations poised in the S_2 and the S_3 states. This implies that manganese is not oxidized during this S-state transition. The similarity of the preedge transition (1s $\rightarrow$ 3d), in amplitude and shape, suggests that the site symmetry and oxidation state are essentially unchanged during the $S_2 \rightarrow S_3$ transition. This evidence and the disappearance of the multiline signal associated with the manganese complex are suggestive that the oxidative equivalent stored on the donor side of PSII during the $S_2 \rightarrow S_3$ state transition is not stored within the manganese complex but is stored on another intermediate magnetically coupled to the manganese complex.

(3) EXAFS analyses indicate that a small structural rearrangement occurs during the $S_2 \rightarrow S_3$ state transition and that an adamantane-like tetranuclear structure is not a reasonable site model for the S_3 state.

(4) Fine adjustments to the EXAFS simulation parameters based on inorganic models imply the presence of two di-μ-oxo-bridged binuclear complexes in the oxygen-evolving complex of PSII. The absence of a change in the Mn K-edge, the disappearance of the multiline signal associated with manganese, and the increase in the disorder in the Mn scattering shell of the EXAFS of PSII together suggest a mechanism of action in which the oxidation of an intermediate donor directly bonded to one of two binuclear complexes results in a small change in the Mn–Mn distance in that complex during the $S_2 \rightarrow S_3$ state transition. Likely aromatic species found in PSII that could serve this function are quinones, tyrosine, histidine, or tryptophan residues.

Acknowledgments

We thank John Vincent, John Bashkin, and Dr. George Christou for generous gifts of many of the multinuclear manganese complexes examined in this study. We are grateful to Dr. Joseph Jaklevic for assistance with the solid-state X-ray detection system used in the collection of the Mn EXAFS. We thank Vickie DeRose for reading the manuscript and for assistance in data acquisition. We thank Dr. Jêrôme Lavergne and Dr. G. T. Babcock for providing manuscripts prior to publication. We would also like to thank the staff at the Stanford Synchrotron Radiation Laboratory for their assistance.

Registry No. **1**, 49729-96-6; **2**, 118867-62-2; **3**, 112988-05-3; **4**, 109170-42-5.

References

Babcock, G. T. (1987) in *New Comprehensive Biochemistry: Photosynthesis* (Amesz, J., Ed.) p 125–158, Elsevier, Amsterdam.

Baumgarten, M., Tso, J., Marino, J., Sivaraja, M., Lin, C. P., Dismukes, G. C., Sheats, J. E., Gast, P., & Philo, J. S. (1989) in *Proceedings of the VIIIth International Congress on Photosynthesis*, Stockholm (in press).

Boussac, A., Zimmermann, J.-L., & Rutherford, A. W. (1989) *Biochemistry, 28*, 8984–8989.

Brown, G. S., & Eisenberger, P. (1979) *Solid State Commun. 29*, 481–484.

Brudvig, G. W., & Crabtree, R. H. (1986) *Proc. Natl. Acad. Sci. U.S.A. 83*, 4586–4588.

Brudvig, G. W., Casey, J. L., & Sauer, K. (1983) *Biochim. Biophys. Acta 723*, 366–371.

Casey, J. L., & Sauer, K. (1984) *Biochim. Biophys. Acta 806*, 21–28.

Coffman, R. E., & Buettner, G. R. (1979) *J. Phys. Chem. 83*, 2387–2392.
Cooper, S. R., & Calvin, M. (1977) *J. Am. Chem. Soc. 99*, 6623–6630.
Cooper, S. R., Dismukes, G. C., Klein, M. P., & Calvin, M. (1978) *J. Am. Chem. Soc. 100*, 7248–7252.
Cramer, S. P., Eccles, T. K., Kutzler, F., Hodgson, K. O., & Doniach, S. (1976) *J. Am. Chem. Soc. 98*, 8059–8069.
Debus, R. J., Barry, B. A., Babcock, G. T., & McIntosh, L. (1988a) *Proc. Natl. Acad. Sci. U.S.A. 85*, 427–430.
Debus, R. J., Barr, B. A., Sithole, I., Babcock, G. T., & McIntosh, L. (1988b) *Biochemistry 27*, 9071–9074.
Dekker, J. P., Van Gorkom, H. J., Wensink, J., & Ouwehand, L. (1984) *Biochim. Biophys. Acta 767*, 209–216.
de Paula, J., C., Innes, J. B., & Brudvig, G. W. (1986) *Biochemistry 24*, 8114–8120.
Dismukes, G. C., & Siderer, Y. (1981) *Proc. Natl. Acad. Sci. U.S.A. 78*, 274–278.
Eisenberger, P., & Kincaid, B. M. (1978) *Science 200*, 1441–1447.
Eisenberger, P., & Lengeler, B. (1980) *Phys. Rev. B 21*, 4507–4520.
Ernst, R. R., Bodenhausen, G., & Wokaun, A. (1987) *Principles of Nuclear Magnetic Resonance in One and Two Dimensions*, pp 150–151, Clarendon Press, Oxford.
George, G. N., Prince, R. C., & Cramer, S. (1989) *Science 243*, 789–791.
Goodin, D. B., Falk, K.-E., Wydrzynski, T., & Klein, M. P. (1979) 6th Annual Stanford Synchrotron Radiation Laboratory Users Group Meetings; SSRL Report No. 79105, pp 10–11.
Goulding, F. S., Landis, D. A., & Madden, N. W. (1983) *IEEE Trans. Nucl. Sci. 30*, 301–310.
Guiles, R. D. (1988) Ph.D. Thesis University of California, Berkeley, CA; Lawrence Berkeley Laboratory Report No. LBL-25186.
Guiles, R. D., Yachandra, V. K., McDermott, A. E., Britt, R. D., Dexheimer, S. L., Sauer, K., & Klein, M. P. (1987) in *Progress in Photosynthesis Research* (Biggins, J., Ed.) Vol. 1, pp 73–76, Martinus Nijhoff, Dordrecht.
Ikegami, I., & Katoh, S. (1973) *Plant Cell. Physiol. 14*, 824–836.
Jaklevic, J., Kirby, J. A., Klein, M. P., Robertson, A. S., Brown, G., & Eisenberger, P. (1977) *Solid State Commun. 23*, 679–682.
Joliot, P., Barbieri, G., & Chabaud, R. (1969) *Photochem. Photobiol. 10*, 309–329.
Kirby, J. A., Robertson, A. S., Smith, J. P., Thompson, A. C., Cooper, S. R., & Klein, M. P. (1981) *J. Am. Chem. Soc. 103*, 5529–5537.
Kok, B., Forbush, B., & McGloin, M. (1970) *Photochem. Photobiol. 11*, 457–476.
Kretschmann, H., Dekker, J. P., Saygin, Ö., & Witt, H. T. (1988) *Biochim. Biophys. Acta 932*, 358–361.
Krishtalik, L. I. (1986) *Biochim. Biophys. Acta 849*, 162–171.
Lavergne, J. (1985) *Photochem. Photobiol. 43*, 311–317.
Lavergne, J. (1987) *Biochim. Biophys. Acta 894*, 91–107.
Li, X., Kessissoglou, D. P., Kirk, M. K., Christopher, J. B., & Pecoraro, V. L. (1988) *Inorg. Chem. 27*, 3–5.
McDermott, A. E., Yachandra, V. K., Guiles, R. D., Cole, J. L., Dexheimer, S. L., Britt, R. D., Sauer, K., & Klein, M. P. (1988) *Biochemistry 27*, 4021–4031.
Petrouleas, V., & Diner, B. A. (1986) *Biochim. Biophys. Acta 851*, 416–423.
Petrouleas, V., & Diner, B. A. (1987) *Biochim. Biophys. Acta 893*, 126–137.
Plaksin, P. M., Stoufer, R. C., Mathew, M., & Palenik, G. (1972) *J. Am. Chem. Soc. 94*, 2121–2122.
Powers, L. (1982) *Biochim. Biophys. Acta 683*, 1–38.
Powers, L., Chance, B., Ching, Y., & Angiolillo, P. (1981) *Biophys. J. 34*, 465–498.
Rutherford, A. W., & Zimmermann, J. L. (1984) *Biochim. Biophys. Acta 767*, 168–175.
Rutherford, A. W., & Styring, S. (1987) in *Cytochrome Systems: Molecular Biology and Bioenergetics* (Papa, S., Chance, B., & Ernster, L., Eds.) pp 541–547, Plenum, New York.
Sauer, K., Guiles, R. D., McDermott, A. E., Cole, J. L., Yachandra, V. K., Zimmermann, J.-L., Klein, M. P., Dexheimer, S. L., & Britt, R. D. (1988) *Chem. Scr. 28A*, 87–91.
Sheats, J. E., Czernuszewicz, R. S., Dismukes, G. C., Rheingold, A. L., Petrouleas, V., Stubbe, J., Armstrong, W. H., Beer, R. H., & Lippard, S. (1987) *J. Am. Chem. Soc. 109*, 1435–1444.
Shulman, R. G., Yafet, Y., Eisenberger, P., & Blumberg, W. E. (1976) *Proc. Natl. Acad. Sci. U.S.A. 73*, 1384–1388.
Sivaraja, M., Goodin, D. B., Smith, M., & Hoffman, B. M. (1989) *Science 245*, 738–740.
Srinivasan, A. N., & Sharp, R. R. (1986) *Biochim. Biophys. Acta 850*, 211–217.
Stebler, M., Ludi, A., & Burgi, H.-B. (1986) *Inorg. Chem. 25*, 4743–4750.
Stern, E. A., & Heald, S. M. (1979) *Rev. Sci. Instrum. 50*, 1579–1582.
Styring, S., & Rutherford, A. W. (1988) *Biochim. Biophys. Acta 933*, 378–387.
Takahashi, Y., & Satoh, K. (1987) in *Progress in Photosynthesis Research* (Biggins, J., Ed.) Vol. 2, pp 73–76, Martinus Nijhoff, Dordrecht.
Teo, B.-K. (1986) *EXAFS: Basic Principles and Data Analysis*, pp 1–347, Springer, Verlag, New York.
Teo, B.-K. & Lee, P. A. (1979) *J. Am. Chem. Soc. 101*, 2815–2832.
Teo, B.-K., Antonio, M. R., & Averill, B. A. (1983) *J. Am. Chem. Soc. 105*, 3751–3762.
Vincent, J. B., & Christou, G. (1986) *FEBS Lett. 207*, 250–252.
Vincent, J. B., Christmas, C., Huffman, J. C., Christou, G., Chang, H.-R., & Hendrickson, D. N. (1987) *J. Chem. Soc., Chem. Commun.*, 236–238.
Wieghardt, K., & Bossek, U. (1983) *Angew. Chem., Int. Ed. Engl. 22*, 328–329.
Woolery, G. L., Powers, L., Winkler, M., Solomon, E. I., & Spiro, T. G. (1984) *J. Am. Chem. Soc. 106*, 86–92.
Yachandra, V. K., Guiles, R. D., McDermott, A., Britt, R. D., Dexheimer, S. L., Sauer, K., & Klein, M. P. (1986) *Biochim. Biophys. Acta. 850*, 333–342.
Yachandra, V. K., Guiles, R. D., McDermott, A. E., Cole, J. L., Britt, R. D., Dexheimer, S. L., Sauer, K., & Klein, M. P. (1987) *Biochemistry 26*, 5974–5981.
Zimmermann, J. L., & Rutherford, A. W. (1986) *Biochim. Biophys. Acta 851*, 416–423.